NeuroImage 200 (2019) 101–120

Contents lists available at ScienceDirect

NeuroImage

journal homepage: www.elsevier.com/locate/neuroimage

Detecting resting-state brain activity using OEF-weighted imaging

Yang Yang [a,b,1], Yayan Yin [c,d,1], Jie Lu [c,d,*], Qihong Zou [b,**], Jia-Hong Gao [a,b,e,f,g,***]

[a] Beijing City Key Lab for Medical Physics and Engineering, Institution of Heavy Ion Physics, School of Physics, Peking University, Beijing, 100871, China
[b] Center for MRI Research, Academy for Advanced Interdisciplinary Studies, Peking University, Beijing, 100871, China
[c] Department of Radiology, Xuanwu Hospital, Capital Medical University, Beijing, 100053, China
[d] Beijing Key Laboratory of Magnetic Resonance Imaging and Brain Informatics, Beijing, 100053, China
[e] McGovern Institute for Brain Research, Peking University, Beijing, 100871, China
[f] Shenzhen Key Laboratory of Affective and Social Cognitive Science, Institute of Affective and Social Neuroscience, Shenzhen University, Shenzhen, 518060, China
[g] Shenzhen Institute of Neuroscience, Shenzhen, 518057, China

ARTICLE INFO

Keywords:
Resting state
OEF
Networks
ReHo
fALFF
Test-retest reliability

ABSTRACT

Traditional resting-state functional magnetic resonance imaging (fMRI) is mainly based on the blood oxygenation level-dependent (BOLD) contrast. The oxygen extraction fraction (OEF) represents an important parameter of brain metabolism and is a key biomarker of tissue viability, detecting the ratio of oxygen utilization to oxygen delivery. Investigating spontaneous fluctuations in the OEF-weighted signal is crucial for understanding the underlying mechanism of brain activity because of the immense energy budget during the resting state. However, due to the poor temporal resolution of OEF mapping, no studies have reported using OEF contrast to assess resting-state brain activity. In this fMRI study, we recorded brain OEF-weighted fluctuations for 10 min in healthy volunteers across two scanning visits, using our recently developed pulse sequence that can acquire whole-brain voxel-wise OEF-weighted signals with a temporal resolution of 3 s. Using both group-independent component analysis and seed-based functional connectivity analysis, we robustly identified intrinsic brain networks, including the medial visual, lateral visual, auditory, default mode and bilateral executive control networks, using OEF contrast. Furthermore, we investigated the resting-state local characteristics of brain activity based on OEF-weighted signals using regional homogeneity (ReHo) and fractional amplitude of low-frequency fluctuations (fALFF). We demonstrated that the gray matter regions of the brain, especially those in the default mode network, showed higher ReHo and fALFF values with the OEF contrast. Moreover, voxel-wise test-retest reliability comparisons across the whole brain demonstrated that the reliability of resting-state brain activity based on the OEF contrast was moderate for the network indices and high for the local activity indices, especially for ReHo. Although the reliabilities of the OEF-based indices were generally lower than those based on BOLD, the reliability of OEF-ReHo was slightly higher than that of BOLD-ReHo, with a small effect size, which indicated that OEF-ReHo could be used as a reliable index for characterizing resting-state local brain activity as a complement to BOLD. In conclusion, OEF can be used as an effective contrast to study resting-state brain activity with a medium to high test-retest reliability.

1. Introduction

There has been growing interest in studying resting-state brain activity (Biswal et al., 2010; Fox and Raichle, 2007). In contrast to task-induced brain activity, resting-state functional magnetic resonance imaging (fMRI) detects the intrinsic spontaneous fluctuations of signals. A set of brain regions that are generally referred to as the default mode network (DMN), including the posterior cingulate cortex (PCC) and medial prefrontal cortex (MPFC), decrease their activity during goal-directed tasks but exhibit high cerebral blood flow (CBF) and cerebral metabolic rate of oxygen ($CMRO_2$) in the resting state. Quantitative measurements of the oxygen extraction fraction (OEF) using positron

* Corresponding author. Department of Radiology, Xuanwu Hospital, Capital Medical University, Beijing, 100053, China.
** Corresponding author. Center for MRI Research, Peking University, Beijing, 100871, China.
*** Corresponding author. Center for MRI Research, Peking University, Beijing, 100871, China.
E-mail addresses: imaginglu@hotmail.com (J. Lu), zouqihong@pku.edu.cn (Q. Zou), jgao@pku.edu.cn (J.-H. Gao).
[1] These authors contributed equally to this work.

https://doi.org/10.1016/j.neuroimage.2019.06.038
Received 26 July 2018; Received in revised form 3 June 2019; Accepted 17 June 2019
Available online 19 June 2019

emission tomography (PET) showed that the OEF was spatially uniform during the resting state, and a default mode hypothesis of baseline activity was proposed based on OEF observations (Raichle et al., 2001). Further functional connectivity (FC) analysis has shown that regions in the DMN are functionally intercorrelated during rest (Greicius et al., 2003). Moreover, these DMN regions exhibit high local activity including regional homogeneity (ReHo) (Zang et al., 2004) and fractional amplitude of low-frequency fluctuations (fALFF) (Zou et al., 2008). There are several resting-state brain networks that support visual, auditory and cognitive functions (Beckmann et al., 2005; Damoiseaux et al., 2006; De Luca et al., 2006; Salvador et al., 2005). Studies have shown that alterations of resting-state activity in these brain networks are associated with various psychiatric and neurological disorders (Menon, 2011; Zhou et al., 2008). Resting-state fMRI, with its high spatial resolution and its ability to detect brain activity without task engagement, has been a prominent method used to study basic neuroscience, diagnose brain diseases and monitor treatment outcomes.

Resting-state brain activity studies are mainly based on the blood oxygen level-dependent (BOLD) signal. However, the BOLD signal is a combination of multiple hemodynamic parameters, including CBF, cerebral blood volume (CBV) and $CMRO_2$ (Ogawa et al., 1993), and it may be difficult to interpret without understanding the complex interplay among these parameters. Thus, investigations of resting-state brain activity using signals with clear physiological significance could more directly reveal the basic mechanisms of brain activity. CBF, CBV and $CMRO_2$ are all single physiological parameters. Based on the arterial spin labeling (ASL) technique (Detre et al., 1992), CBF-weighted fluctuations have been used to investigate resting-state brain activity, and the results supported the idea that DMN brain regions play a vital role in maintaining and facilitating basic brain functions (Zou et al., 2009). The results of spontaneous CBV-weighted fluctuations using a vascular space occupancy (VASO) imaging technique (Lu et al., 2003) showed that the brain regions that suffered from BOLD signal loss tended to have less geometric distortion in VASO-based signals, which suggests that CBV may become an attractive approach for studying brain functions in regions where BOLD contrast is not suitable (Miao et al., 2014). Based on a biophysical model (Davis et al., 1998), the synchronized $CMRO_2$--weighted fluctuations in the resting state were investigated, and the results indicated that spontaneous fMRI signal fluctuations have a metabolic origin (Wu et al., 2009a,b). OEF is also a single physiological parameter with an explicit physiological meaning. Thus, investigations of the spontaneous fluctuations of OEF-weighted signals in the resting state are crucial to interpreting the signal changes associated with brain metabolism, which may lead to an improved understanding of brain physiology.

OEF is defined as the ratio of oxygen consumption to oxygen delivery by flowing blood, reflecting the amount of oxygen that leaves the blood stream to enter surrounding tissues. Because oxidative metabolism is the principal way in which energy is supplied to the brain, OEF offers a more direct assessment of metabolic changes than BOLD signals (Stout et al., 2018). However, due to the low temporal resolution of OEF mapping, previous studies on OEF measurements were mostly quantitative and static (Bush et al., 2018; He and Yablonskiy, 2007; Hyder et al., 2016; Merola et al., 2018). No study has detected resting-state networks or local brain characteristics based on OEF-weighted fluctuations across time. Recently, the multiecho asymmetric spin echo (MASE) pulse sequence was proposed for mapping OEF-weighted fluctuations and was verified by a human motor task paradigm (Yin et al., 2018). The MASE sequence greatly improves the temporal resolution of OEF measurements, and it is feasible to map whole-brain voxel-wise OEF-weighted signals within 3 s. Thus, the first goal of the current study was to detect OEF-based resting-state brain networks and local brain characteristics using the MASE sequence.

Furthermore, test-retest reliability evaluation is very important for brain activity measures (Jahng et al., 2005; Jann et al., 2015a; Patriat et al., 2013a; Zhu et al., 2014). Previous investigations on the test-retest reliability of spontaneous BOLD signal oscillations (Küblböck et al., 2014; Zuo et al., 2010b) showed that the brain regions with moderate to high reliability of FC and local characteristics were mainly located in the gray matter. Similar results were observed in several studies investigating the test-retest reliability of average CBF (Hodkinson et al., 2013a; Jahng et al., 2005; Jann et al., 2015a; Zou et al., 2015). The second goal was to evaluate whether OEF could be used as a reliable signal contrast to detect resting-state human brain activity.

In the present study, resting-state brain networks and local characteristics were investigated, based on both whole-brain OEF-weighted fluctuations using the MASE sequence and BOLD signals from the same group of subjects. Group independent component analysis (ICA) and seed-based FC were used to detect the brain networks. Both the ReHo and fALFF indices were used to investigate the local intrinsic brain activity based on OEF-weighted and BOLD signals. Moreover, we evaluated the test-retest reliability of the network and local characteristics based on both OEF and BOLD contrasts. The patterns of OEF-based resting-state brain activity and corresponding test-retest reliability were subsequently compared to those based on BOLD.

2. Materials and methods

2.1. Participants

Twenty-three healthy, right-handed subjects (23.17 ± 2.53 years old, 12 males) participated in this study. Signed informed consent was obtained from each participant prior to study enrollment. This study was approved by the institutional review board of Peking University, Beijing, China.

2.2. Experimental paradigm

Subjects were imaged at two scanning visits approximately one month apart (36.32 ± 0.95 days). For each scanning visit, two resting-state scans (with OEF and BOLD contrasts, respectively), which were taken with the eyes open while looking at a black screen, were acquired for each subject. The order of OEF- and BOLD-contrast resting scans was pseudorandomized among subjects. It should be noted that one subject did not participate in the retest experiments. In the end, four resting-state fMRI scans were acquired for each of the 22 subjects across the two scanning visits.

2.3. Data acquisition

The fMRI data were collected on a 3 T GE Discovery MR750 MRI scanner (GE Healthcare, Milwaukee, WI, USA) equipped with an 8-channel head coil in the Center for MRI Research at Peking University. Foam pads were used to limit head motion, and scanner noise was attenuated by earplugs.

Before fMRI data collection, a high-order shimming sequence was performed to minimize magnetic field inhomogeneity. A MASE sequence based on an echo-planar imaging (EPI) acquisition scheme (Yin et al., 2018) was adopted for OEF-weighted imaging acquisition (Yin et al., 2018). In the MASE sequence, a 90° spectral-spatial excitation pulse was used to excite the imaging volume, which was subsequently refocused by a 180° refocusing pulse. The data were acquired after the 180° pulse with six EPI readout trains (the readout durations were 12.284, 11.772, 11.772, 11.772, 11.772 and 11.772 ms separately). A single-shot gradient-echo EPI sequence was used for BOLD imaging acquisition. The common pulse sequence parameters for both OEF-weighted and BOLD images were as follows: field of view (FOV) = $26 \times 26\ cm^2$; slice thickness/gap = 6 mm/0 mm; repetition time (TR) = 3 s; and matrix size = 64×64. Twenty-two slices were prescribed to cover the whole brain. For OEF-contrast fMRI, a MASE sequence with SENSE factor = 2 and six different echo times (40, 60, 80, 92.412, 104.824, and 117.236 ms) was used to estimate the OEF-weighted images. The echo

time represents the time between the middle of the 90° excitation pulse and the peak of the echo signal for each echo. For BOLD-contrast fMRI, specific acquisition parameters included a flip angle of 90° and an echo time of 30 ms. The total resting-state scanning time was the same (10 min and 30 s) for OEF-weighted and BOLD acquisitions and corresponded to 210 measurements.

A 3D FSPGR sequence was performed to acquire T_1-weighted images that were used as an anatomic reference for better registration (TR/TE/flip angle = 6.6 ms/2.9 ms/12°, voxel size = 1 mm^3 isotropic).

2.4. Data preprocessing

Both the data acquired using MASE (six echoes separately) and a single-shot gradient-echo EPI sequence were preprocessed using the Statistical Parametric Mapping package (SPM, https://www.fil.ion.ucl.ac.uk/spm/software/spm12/) with the following procedures: 1) removal of the first 10 vol; 2) motion correction for head movement during the scan; 3) coregistration of functional images to structural images; 4) spatial normalization to the Montreal Neurological Institute (MNI) standard brain space with a resampled resolution of $3 \times 3 \times 3\ mm^3$ to facilitate group analysis; and 5) spatial smoothing (FWHM = 6 mm) to minimize individual variance.

For MASE data, the voxel-wise OEF-weighted value of each volume was calculated using customized programs written in MATLAB (Mathworks, Natick, MA, USA) based on the preprocessed data for all six echoes. The strategy for detailed calculation of OEF-weighted values has been described in our previous publication (Yin et al., 2018). It should be noted that $\Delta\chi_0$ is the susceptibility difference between fully oxygenated and fully deoxygenated blood (Yin et al., 2018), and we adopted 0.27 ppm as the $\Delta\chi_0$ value when calculating the OEF-weighted value.

It should be noted that the data from three subjects were discarded because the head motion exceeded a displacement of 2 mm or a rotation of 2°. Twenty subjects were included in the subsequent group ICA, FC, ReHo and fALFF analyses. Eighteen of the 20 subjects (one was absent, and the head motion of the other exceeded a 2 mm displacement or a 2° rotation) who successfully completed the retest study were included in test-retest reliability analyses.

2.5. Data analysis

2.5.1. Group ICA of OEF and BOLD

To identify resting functional networks, we applied group ICA to OEF-weighted and BOLD resting fMRI data separately, using the MELODIC tool in the FMRIB Software Library (FSL, https://fsl.fmrib.ox.ac.uk/fsl/fslwiki). After the linear detrending of signal drift, grand-mean intensity normalization and high-pass temporal filtering with a cutoff value of 100 s, the preprocessed data from the 20 subjects were concatenated in the temporal dimension to form a single data set to be fed into the probabilistic ICA algorithm. The number of components was set at 25. The resting functional networks were visually identified based on their similarity to known brain networks (Calhoun and Adali, 2012; Heine et al., 2012; Smith et al., 2009), and six components were selected as functional networks of interest.

2.5.2. Seed-based FC of OEF and BOLD

Seed-based FC analysis was also performed on the resting-state OEF-weighted and BOLD data for comparison to the group ICA analysis. For the MASE data, regression of the six head motion parameters was performed separately for each echo after spatial normalization. Subsequently, the OEF value of each volume was calculated using customized programs (Yin et al., 2018). Then, the nuisance covariates, including the mean time courses of the white matter and cerebrospinal fluid, were regressed out of the calculated OEF-weighted time series, and spatial smoothing (FWHM = 6 mm) was performed. To generate corresponding connectivity maps, we defined six seed ROIs (10 mm in diameter), located as follows: in the right calcarine sulcus (16, −67, 5) (Elton and Gao, 2015; Gao and Lin, 2012); the right lateral occipital gyrus (37, −85, 13) (Gao and Lin, 2012); the left Heschl's gyrus (−42, −26, 10) (Shinn et al., 2013); the PCC (0, −53, 26) (Yan et al., 2013); the left anterior inferior parietal lobule (−52, −49, 47) (Gao and Lin, 2012; Vincent et al., 2008); and the right anterior inferior parietal lobule (52, −46, 46) (Gao and Lin, 2012; Vincent et al., 2008). After linear trend removal and bandpass filtering (0.01–0.08 Hz), the FC maps were obtained using the Resting-State fMRI Data Analysis Toolkit (REST, http://www.restfmri.net/forum/REST_V1.8) (Song et al., 2011), and one-sample t-tests were performed on individual Fisher's z-maps to determine whether the z-scores were significantly higher than zero. For BOLD-FC analysis, after head motion correction, coregistration, spatial normalization and spatial smoothing (FWHM = 6 mm), the nuisance covariates (six head motion parameters and the mean time courses of the white matter and cerebrospinal fluid) were regressed out. Then, linear trend removal and bandpass filtering (0.01–0.08 Hz) were performed. Finally, the FC maps were calculated using REST based on the same seeds used for OEF-FC, and one-sample t-tests were also performed.

2.5.3. OEF-ReHo and BOLD-ReHo

To detect local synchrony of brain regions, we performed ReHo analysis to measure the similarity of the time courses of the voxels within a given cluster (cubic cluster with 27 voxels in this study). In theory, ReHo assumes that the time courses within a functional cluster are similar to each other; Kendall's coefficient of concordance (KCC) was used to estimate the degree of similarity of multiple time courses. For both OEF and BOLD analyses, after linear detrending and bandpass filtering (0.01–0.08 Hz) based on the preprocessed data after spatial normalization, ReHo maps were calculated using REST. Then, each subject's ReHo map was divided by that subject's global mean ReHo value. Spatial smoothing (FWHM = 6 mm) was performed on the normalized ReHo maps, and one-sided one-sample t-tests against 1 were performed on the smoothed maps for both OEF-weighted and BOLD data.

2.5.4. OEF-fALFF and BOLD-fALFF

Using REST, fALFF, i.e., a ratio of the power in the low-frequency range to that of the entire frequency range, was calculated to detect brain activity based on OEF-weighted and BOLD data. After linear detrending of the preprocessed data, the time courses of each voxel were transformed to a frequency domain without bandpass filtering. After the square root was calculated at each frequency of the power spectrum, the sum of the amplitudes across 0.01–0.08 Hz was divided by that across the entire frequency range. Similar to ReHo analysis, each subject's fALFF map was divided by that subject's global mean fALFF value, and one-sided one-sample t-tests against 1 were then performed on the normalized maps for both OEF-weighted and BOLD data.

2.5.5. Test-retest reliability quantified by intraclass correlation

Intraclass correlation (ICC) was used to examine the test-retest reliability of the resting-state brain activity indices calculated based on OEF-weighted and BOLD fluctuations; ICC is defined as the proportion of variability across subjects relative to the total variability in the data.

$$ICC = (MS_b - MS_w)/(MS_b + (k-1)MS_w) \quad (1)$$

where MS_b is the between-subject mean square, MS_w is the within-subject mean square, and k is the number of observations made on each subject ($k = 2$ for the ICC calculation). ICC has been widely used in neuroimaging studies (Andellini et al., 2015; Hodkinson et al., 2013a; Jann et al., 2015a; Patriat et al., 2013a; Zou et al., 2015). The higher the ICC value is, the lower the within-subject variance relative to the between-subject variance, which suggests higher reliability. Generally, imaging metrics with moderate to high ICC values (≥0.4) are considered reliable for neuroimaging studies (Zuo and Xing, 2014).

To assess the test-retest reliability of the networks based on group ICA, we performed dual regression analysis to derive a component map

for each scanning session and each subject using the following two linear regression steps (Zou et al., 2018). First, each of the spatial component maps derived from the group ICA was regressed against each volume of fMRI data. Then, the resulting spatial regression coefficients were concatenated across time. Second, the variance-normalized time series from the above spatial regressions were regressed against the corresponding resting-state fMRI time course to estimate the regression weights of specific component maps in individual participants.

2.5.6. Comparison of test-retest reliability between different metrics

Histograms of ICC values across the whole brain were used to qualitatively compare the different imaging indices within and between OEF and BOLD contrasts. Subsequently, a series of paired Wilcoxon signed-rank tests were performed to investigate whether the distributions of ICC values were significantly different between the resting-state activity indices and between the two imaging contrasts across the whole brain. The effect size was calculated as:

$$r = Z \Big/ \sqrt{N} \tag{2}$$

where Z is the Z statistic from Wilcoxon's signed-rank test and N is the number of observations; here, $N = 2 \times$ the number of voxels within the whole brain (Zou et al., 2015). Effect sizes were rated as small ($0.3 > r \geq 0.1$), medium ($0.5 > r \geq 0.3$) and large ($r \geq 0.5$).

2.5.7. Functional connectivity and local activity analyses based on all MASE-derived parameters

OEF, vCBV, R2 and R2′-weighted fluctuations can be estimated from MASE-derived signals, and the calculation details have been shown in our previous paper (Yin et al., 2018). The time courses of the estimated OEF, vCBV, R2 and R2′ from the MASE sequence for a typical subject were calculated, and group ICA, seed-based FC, ReHo and fALFF analyses were performed based on OEF, vCBV, R2 and R2′-weighted fluctuations.

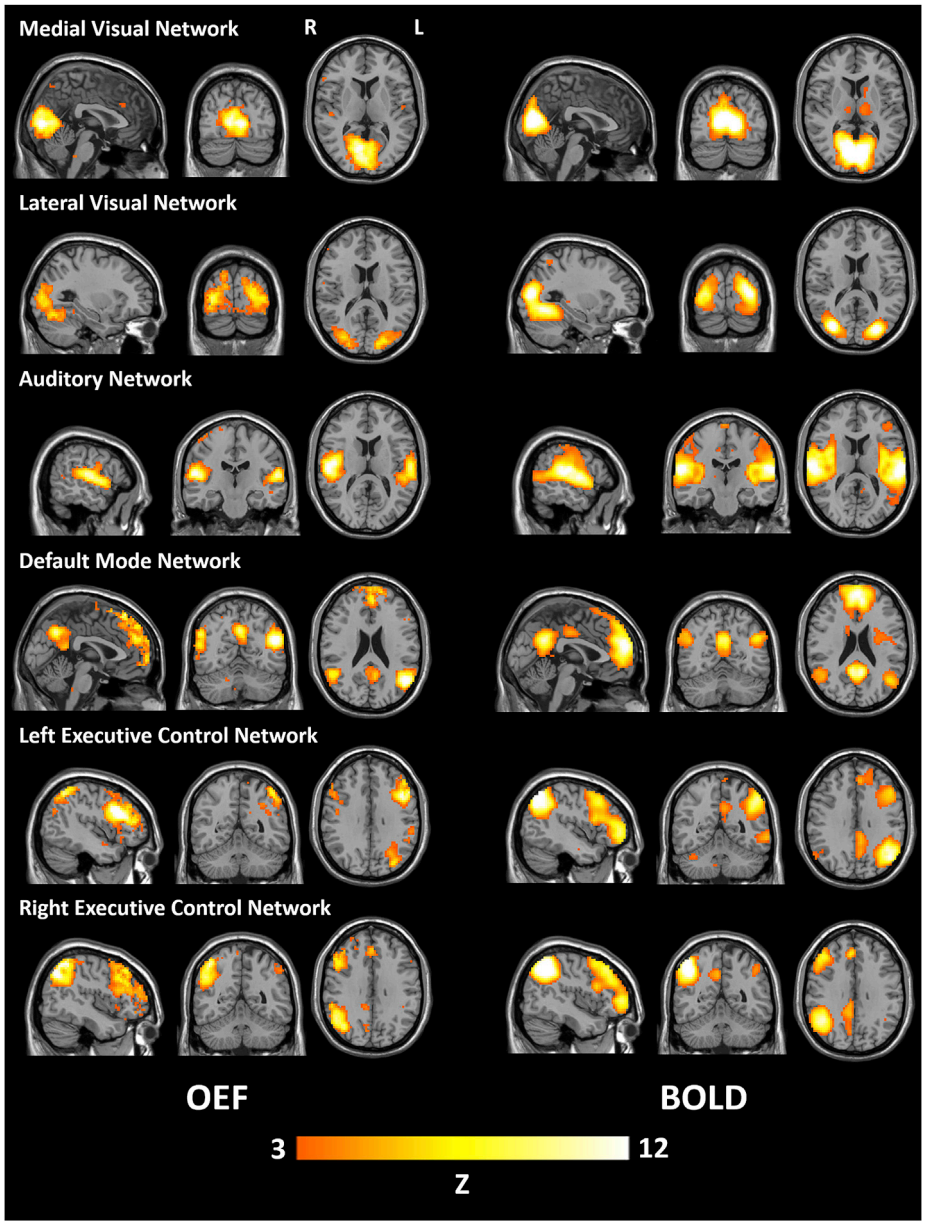

Fig. 1. Functional networks of interest from group ICA of 20 subjects based on the data from the first scan. The medial visual, lateral visual, auditory, default mode and bilateral executive control networks were identified from 25 components for both the OEF and BOLD contrasts. All ICA spatial maps were converted to Z statistic maps via a mixture-model fit and thresholded at $Z > 3$.

3. Results

3.1. Functional networks generated by group ICA and seed-based FC

Six resting functional networks were identified as biologically meaningful out of the 25 components generated by group ICA of the OEF-weighted resting-state data, including the medial visual network, lateral visual network, auditory network, DMN, left executive control network (ECN) and right ECN, as shown in Fig. 1. For comparison, the corresponding functional networks generated from BOLD resting data are also displayed in Fig. 1. All ICA spatial maps were converted to Z statistic maps via a normalized mixture-model fit and thresholded at $Z > 3$. The brain regions included in the thresholded OEF-based functional network maps are summarized as follows. The medial visual network encompassed the bilateral calcarine sulcus, bilateral cuneus, and bilateral lingual gyrus. The lateral visual network included the middle temporal visual association area towards the temporo-occipital junction. The auditory network encompassed the bilateral superior temporal gyrus, bilateral Heschl's gyrus and bilateral rolandic operculum. The DMN covered the PCC, MPFC, bilateral precuneus and bilateral angular gyrus. The left ECN and right ECN encompassed the unilateral inferior parietal lobule, superior parietal lobule, inferior frontal cortex and middle frontal cortex. There were some differences in the network maps between the group ICA results obtained using BOLD and OEF-based data. For example, the brain regions that belonged to the networks were spread wider spatially in the BOLD networks than the OEF-based networks. The percentage of the number of voxels in the gray matter was higher in the OEF-based group ICA results than in the BOLD results (79.41% ± 2.42% versus 74.62% ± 1.65%, respectively, across the six networks).

For the purpose of validating whether the ICA results were stable, the number of components was also separately set to 20 and 30 when performing ICA analysis. The results showed that six networks, including the medial visual network, lateral visual network, auditory network, DMN, left ECN and right ECN, could be robustly identified after ICA

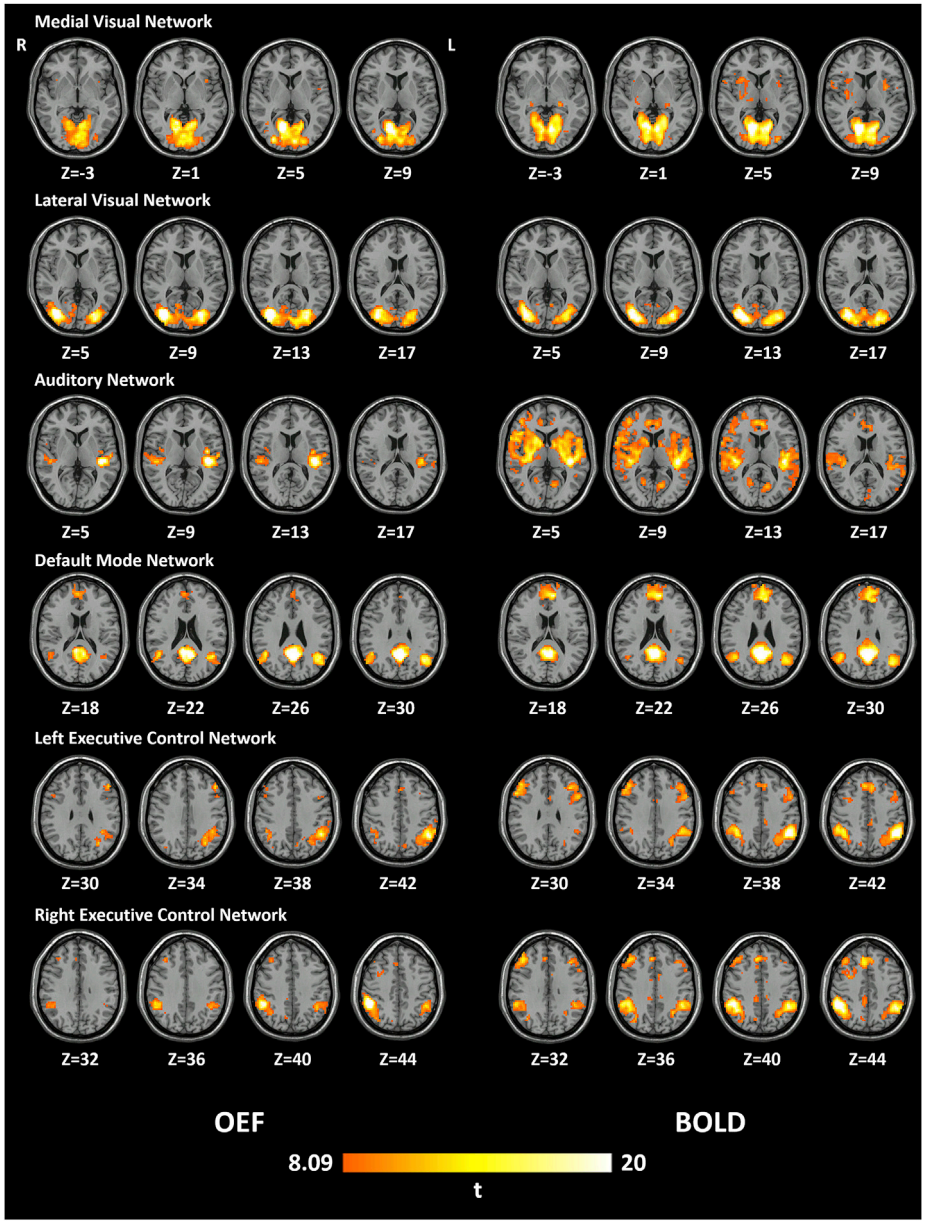

Fig. 2. Seed-based FC maps of 20 subjects based on the data from the first scan. The numbers below the maps are Z coordinates in the axial view in MNI space. These networks include the medial visual, lateral visual, auditory, default mode and bilateral executive control networks. The connectivity maps were thresholded at voxel-level FWE correction of $p < 0.005$.

decomposition at dimensionalities of both 20 and 30 (as shown in Figs. S1 and S2 in the Supplementary Materials), which suggested that the six OEF-based networks from the ICA analysis were negligibly affected by dimensionality during ICA decomposition.

Seed-based FC analysis of the OEF-weighted and BOLD data produced similar network maps, as shown in Fig. 2 (the OEF- and BOLD-based connectivity maps shown were both thresholded at a voxel-level familywise error (FWE) correction of $p < 0.005$). The network patterns of the OEF-based and BOLD-based data were similar; however, differences still existed in the network maps. Similar to the ICA results, the seed-based FC maps based on BOLD data included spatially larger and more numerous brain regions than those based on OEF-weighted fluctuations; however, the OEF-FC maps showed potentially more accurate spatial locations, which appeared to be more localized in the gray matter, while the BOLD-FC maps tended to spread to the neighboring white matter. The percentage of the number of voxels in the gray matter was higher in the OEF-FC results than in the BOLD results ($82.96\% \pm 4.25\%$ versus $78.90\% \pm 2.47\%$, respectively).

3.2. ReHo and fALFF spatial patterns

The brain regions that showed higher local synchrony than the global average for the OEF and BOLD contrasts are shown in Fig. 3 (voxel-level $p < 0.001$ with a cluster-level false discovery rate (FDR) correction of $p < 0.05$ using SPM). The PCC, MPFC, bilateral angular gyrus, bilateral precuneus and bilateral cuneus had higher local synchrony than other brain regions for both the OEF and BOLD contrasts.

The fALFF results for both the OEF and BOLD contrasts showed that the PCC, MPFC, bilateral middle frontal gyrus, angular gyrus, precuneus and cuneus had higher fALFF values than the whole-brain average, as shown in Fig. 4 (voxel-level $p < 0.001$ with a cluster-level FDR correction of $p < 0.05$). In addition to the DMN regions, other gray matter regions, including the superior temporal gyrus, middle temporal gyrus, rolandic operculum, middle frontal gyrus, inferior frontal gyrus, precentral gyrus, postcentral gyrus, cerebellar posterior lobe and cerebellar anterior lobe, also showed higher fALFF values for the OEF contrast.

The correction methods used in the ReHo and fALFF analyses were different from those used in the seed-based FC analysis. When using the

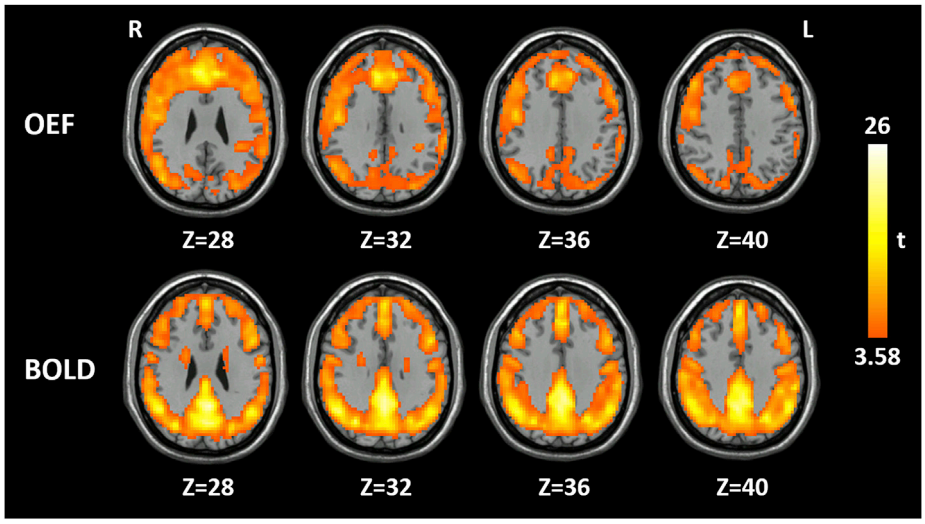

Fig. 3. ReHo maps of 20 subjects based on the data from the first scan. The numbers below the maps are Z coordinates in the axial view in MNI space. The results from a one-sample *t*-test on the ReHo maps were thresholded at voxel-level $p < 0.001$ with a cluster-level FDR correction of $p < 0.05$.

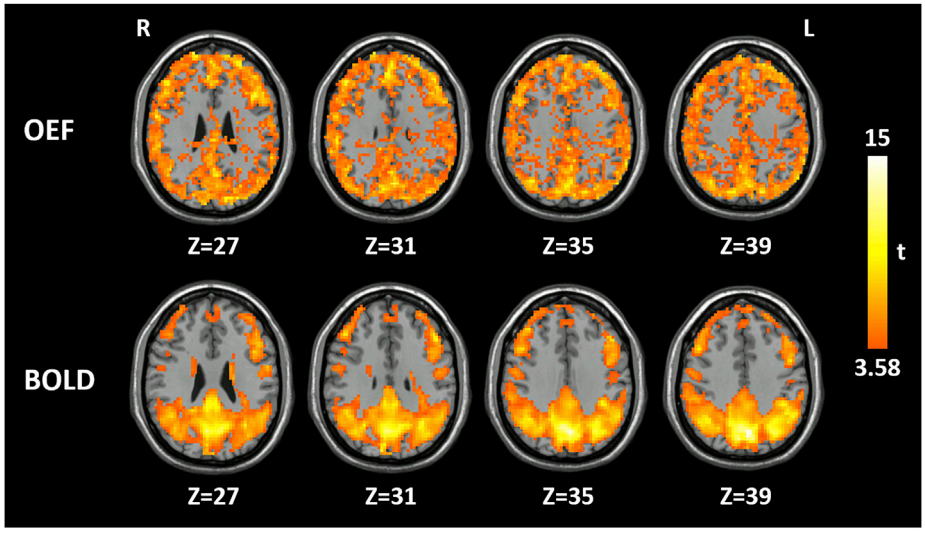

Fig. 4. fALFF maps of 20 subjects based on the data from the first scan. The numbers below the maps are Z coordinates in the axial view in MNI space. The results from a one-sample *t*-test on the fALFF maps were thresholded at voxel-level $p < 0.001$ with a cluster-level FDR correction of $p < 0.05$.

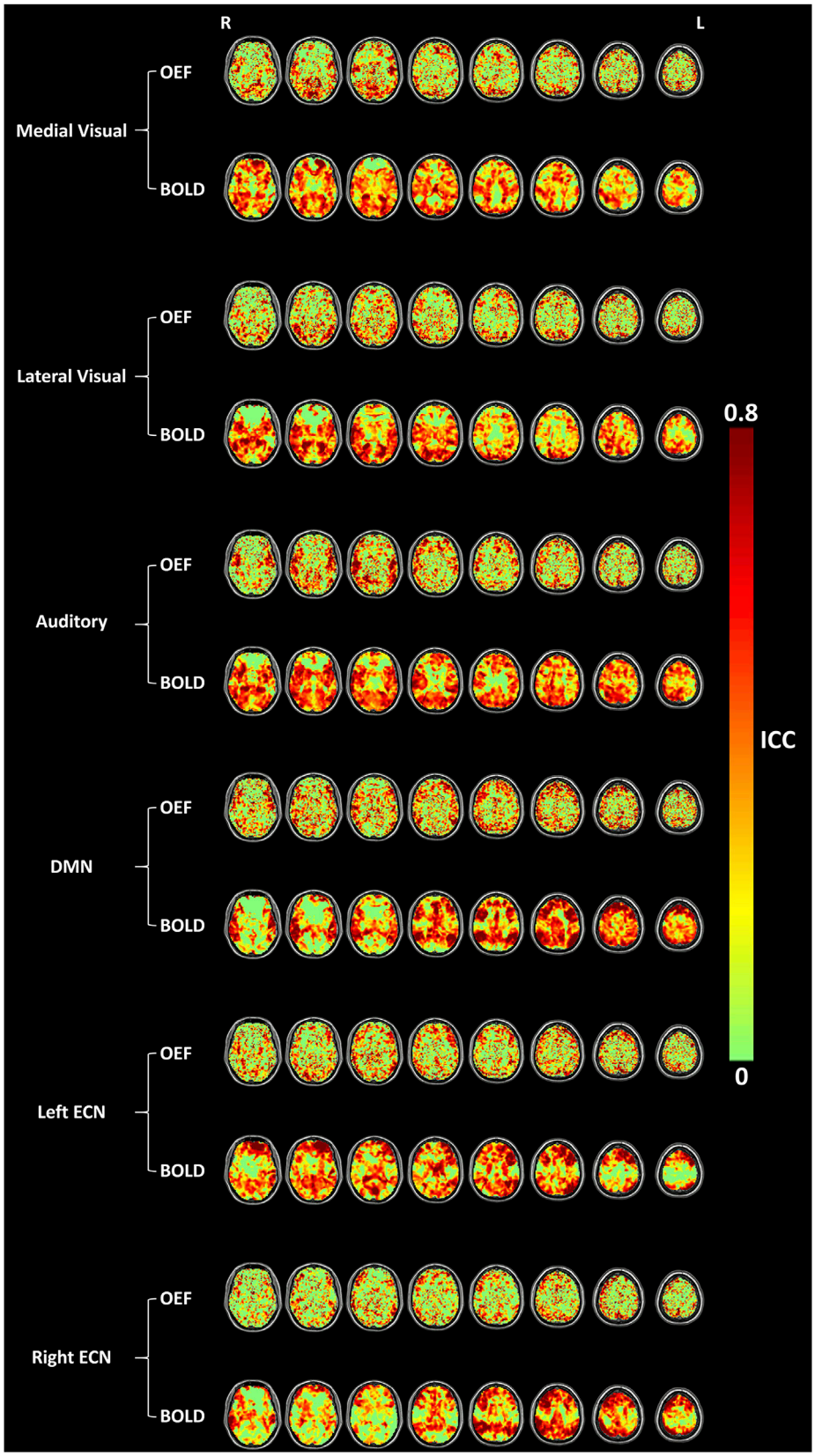

Fig. 5. ICC maps for group ICA. ICC maps of six group ICA components, the medial visual network, lateral visual network, auditory network, DMN and bilateral ECN, computed from both the OEF and BOLD contrasts. Z-axial coordinates in MNI space are from −10 to 60 mm in steps of 10 mm.

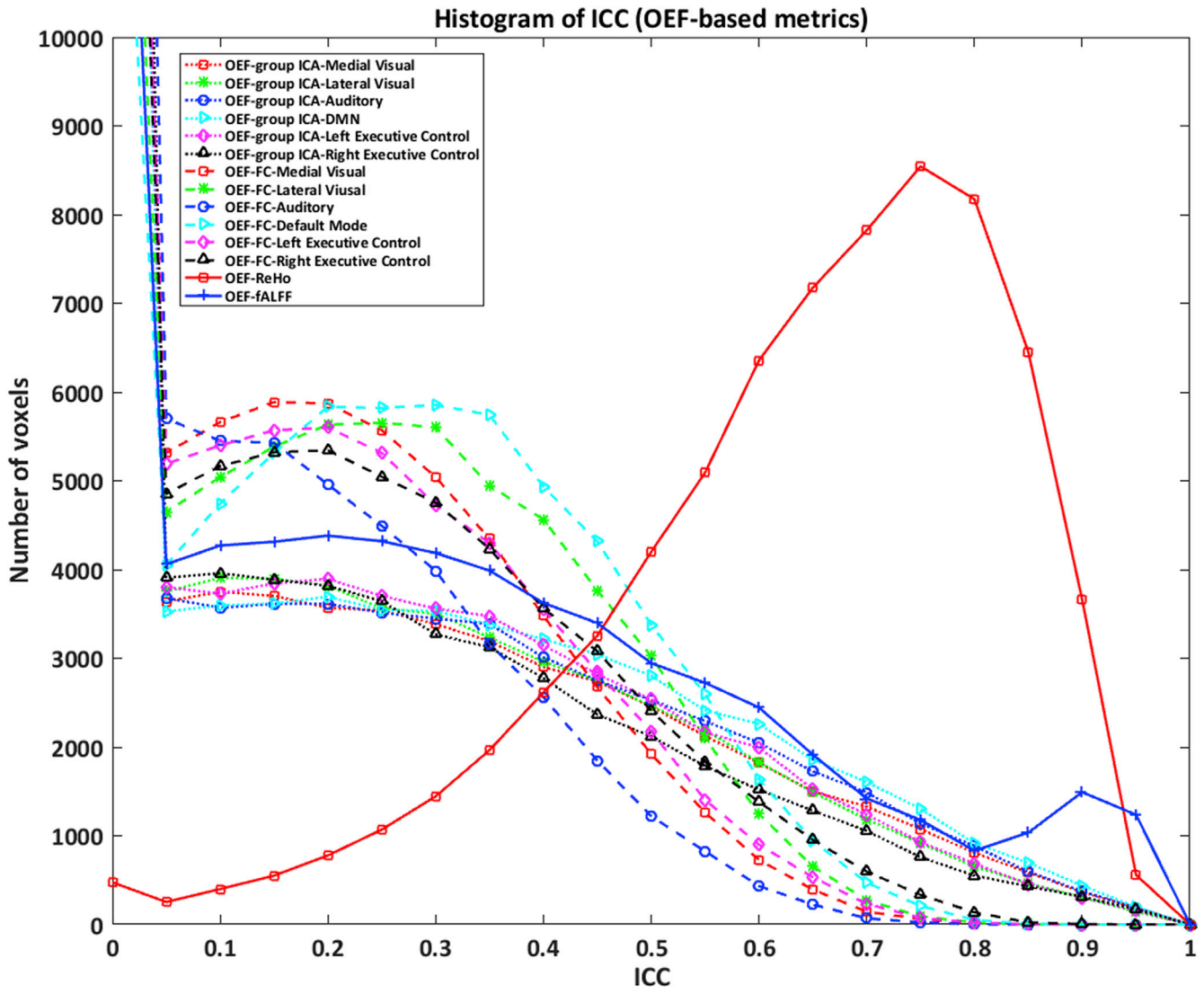

Fig. 6. Histograms of ICC among different OEF-based indices. The dotted lines indicate the six group ICA networks, the medial visual network, lateral visual network, auditory network, DMN and bilateral ECN. The dashed lines indicate the six FC-based networks. The solid lines indicate the ReHo and fALFF.

same correction method (voxel-level $p < 0.001$ with a cluster-level FDR correction of $p < 0.05$), the network patterns for both the OEF and BOLD contrasts included extremely large brain areas comprising both gray matter and white matter (as shown in Fig. S3 in the Supplementary Materials). Thus, a stringent correction method (voxel-level FWE correction of $p < 0.005$) was performed to correct the FC results.

3.3. Test-retest reliability of group ICA, FC, ReHo and fALFF within and between imaging contrasts

We evaluated the reliability of the resting-state activity indices, including group ICA, seed-based FC, ReHo and fALFF, computed using each of the two imaging contrasts. We further compared the reliability of the resting-state activity indices within and between the two contrasts separately.

The brain regions showing high ICC for each OEF-based group ICA component were mainly located in the gray matter regions included in the corresponding networks (Fig. 5). The histograms of the ICC for the six OEF-based group ICA networks showed similar patterns, with moderate test-retest reliability (Fig. 6). For seed-based FC networks based on OEF-weighted fluctuations, the regions with moderate to high ICC were also mainly located in the gray matter regions included in the corresponding networks (Fig. 7). The histograms of ICC of these FC networks showed medium ICC values (Fig. 6). OEF-ReHo exhibited extremely high ICC across the whole gray matter (Fig. 8). OEF-fALFF showed moderate to high ICC in the gray matter (Fig. 8).

Comparison of the ICC histograms (Fig. 6) showed a higher ICC for OEF-ReHo than for other OEF-based indices, with large effect sizes (Fig. 9). The OEF-fALFF had higher reliability than all network indices including the six group ICA components and the six seed-based FC maps with small to medium effect sizes, except for the ICA-based and FC-based DMN (Fig. 9). Comparisons between ICC histograms for each pair of the six ICA-derived networks yielded a minimal effect size, except that DMN-FC showed higher reliability than RECN-FC, which yielded a small effect size (Fig. 9). The DMN-FC generally showed higher reliability than all six ICA-derived networks and the other five seed-based FC maps, while the auditory network based on seed-based connectivity exhibited a lower ICC than other networks (Fig. 9).

The test-retest reliability maps and histograms of the ICC values for the BOLD contrast were similar to those for the OEF contrast and were generally consistent with previous findings (Li et al., 2012; Pannunzi et al., 2017; Shehzad et al., 2009; Zuo et al., 2010a,b, 2013). The ICC histogram patterns of the six BOLD-based group ICA networks and the six seed-based FC networks were similar (Fig. 10). Comparisons between

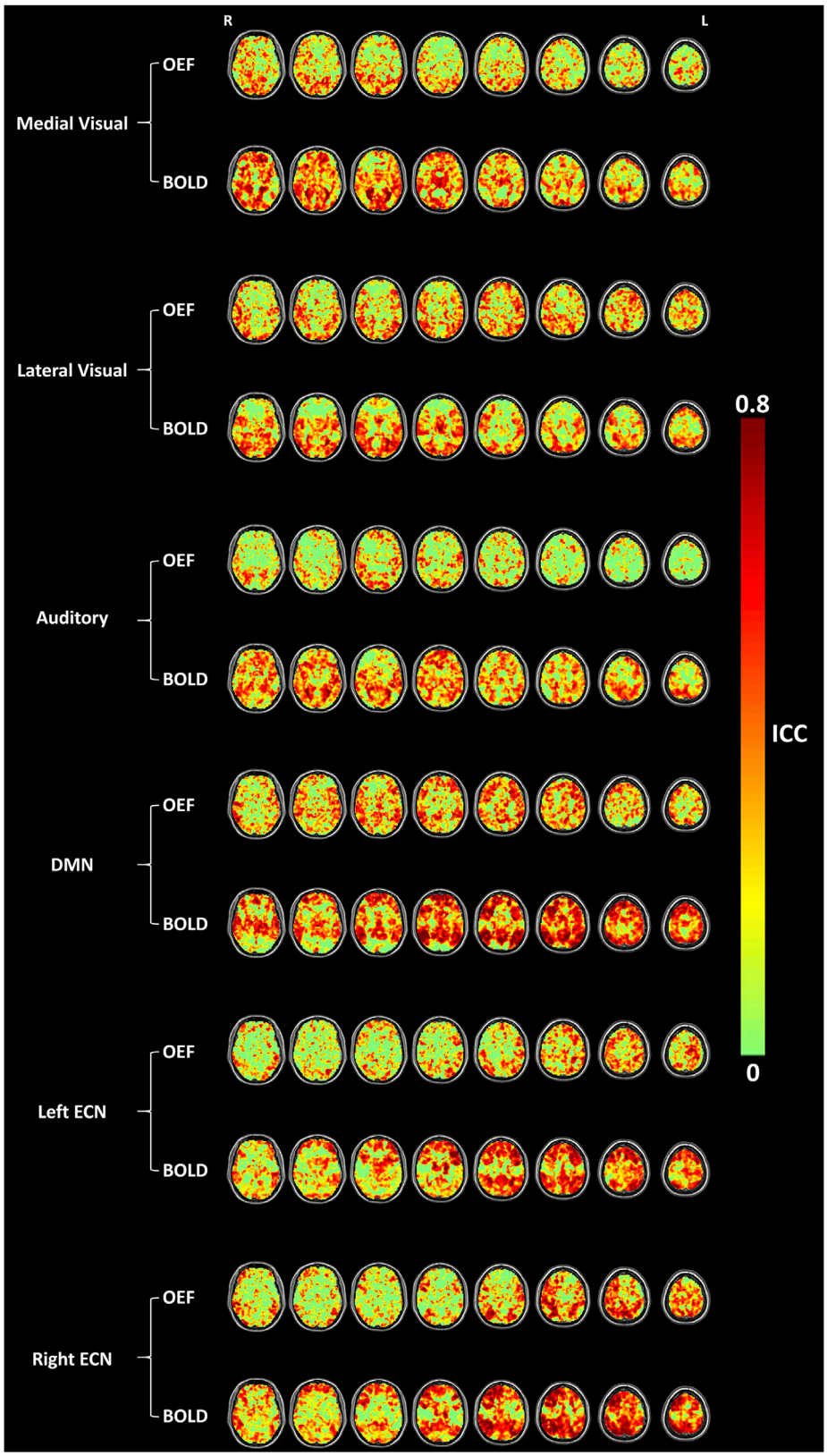

Fig. 7. ICC maps for seed-based FC. ICC maps of six seed-based FC maps, the medial visual network, lateral visual network, auditory network, DMN and bilateral ECN, computed from both the OEF and BOLD contrasts. Z-axial coordinates in MNI space are from −10 to 60 mm in steps of 10 mm.

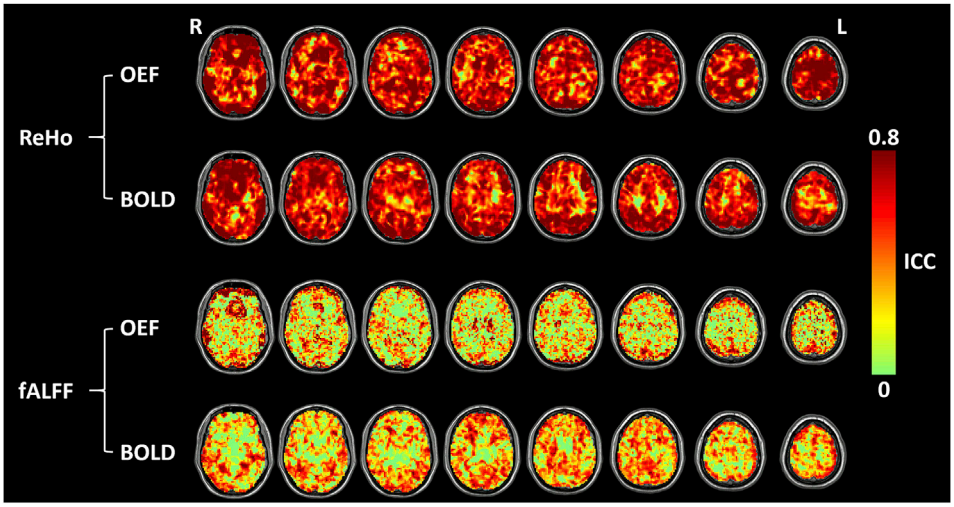

Fig. 8. ICC maps for ReHo and fALFF. ICC maps of ReHo and fALFF computed from two imaging contrasts. Z-axial coordinates in MNI space are from −10 to 60 mm.

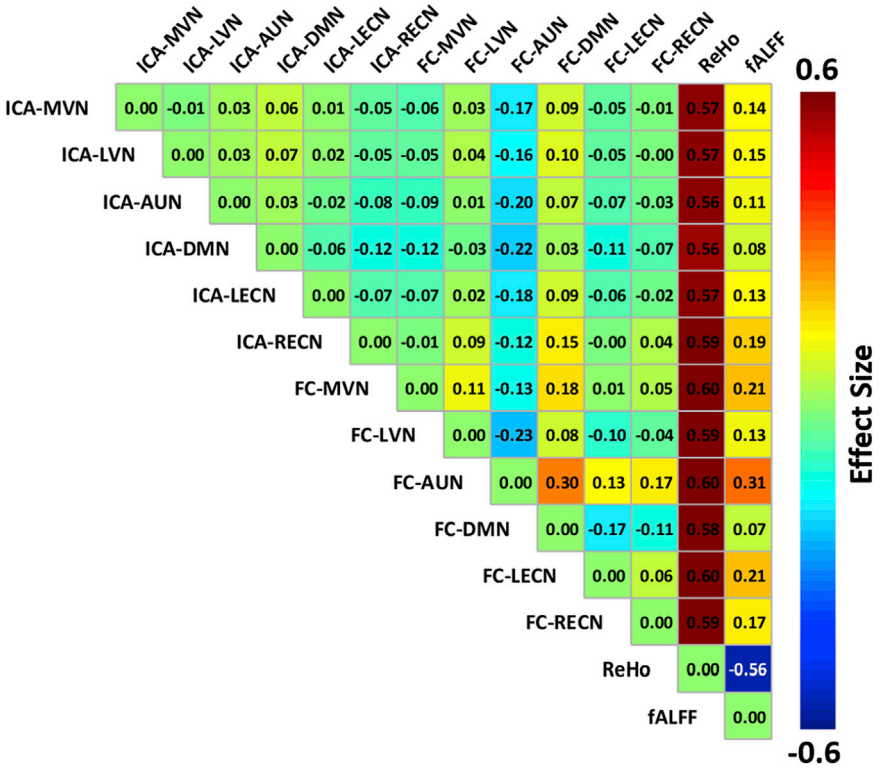

Fig. 9. Effect size of comparisons of ICC histograms between different OEF-based indices. "MVN", "LVN", "AUN", "DMN", "LECN" and "RECN" indicate the medial visual network, lateral visual network, auditory network, default mode network, left ECN and right ECN, respectively. A positive number shown in a small square indicates that the index above this square exhibits a trend of higher reliability than the index to the left of that square, and a negative number represents the opposite effect.

different network indices generally yielded minimal to small effect sizes (Fig. 11). BOLD-ReHo showed higher reliability than all other BOLD-based indices, which yielded medium to large effect sizes (Fig. 11). BOLD-fALFF showed ICC histograms similar to those of network indices based on BOLD, except that its reliability was lower than that of FC-DMN (Fig. 11).

All six OEF-based group ICA networks showed lower reliabilities than the BOLD-based group ICA networks, with small effect sizes (Table 1). Similar to the group ICA results, the six seed-based FC networks based on OEF-weighted fluctuations also showed lower reliabilities than the BOLD-based FC networks, with small to medium effect sizes. It should be noted that the ICC of OEF-ReHo was higher than that of BOLD-ReHo, with a small effect size (Table 1). The ICC of OEF-fALFF indicated lower reliability than BOLD, with a minimal effect size (Table 1).

3.4. Functional connectivity and local activity results based on all MASE-derived parameters

The time courses of the estimated OEF, vCBV, R2 and R2′ from the MASE sequence for a typical subject are shown in Fig. 12, and the percent signal changes of OEF and vCBV were similar to the results in our previous study (Yin et al., 2018). R2′ and vCBV were highly correlated based

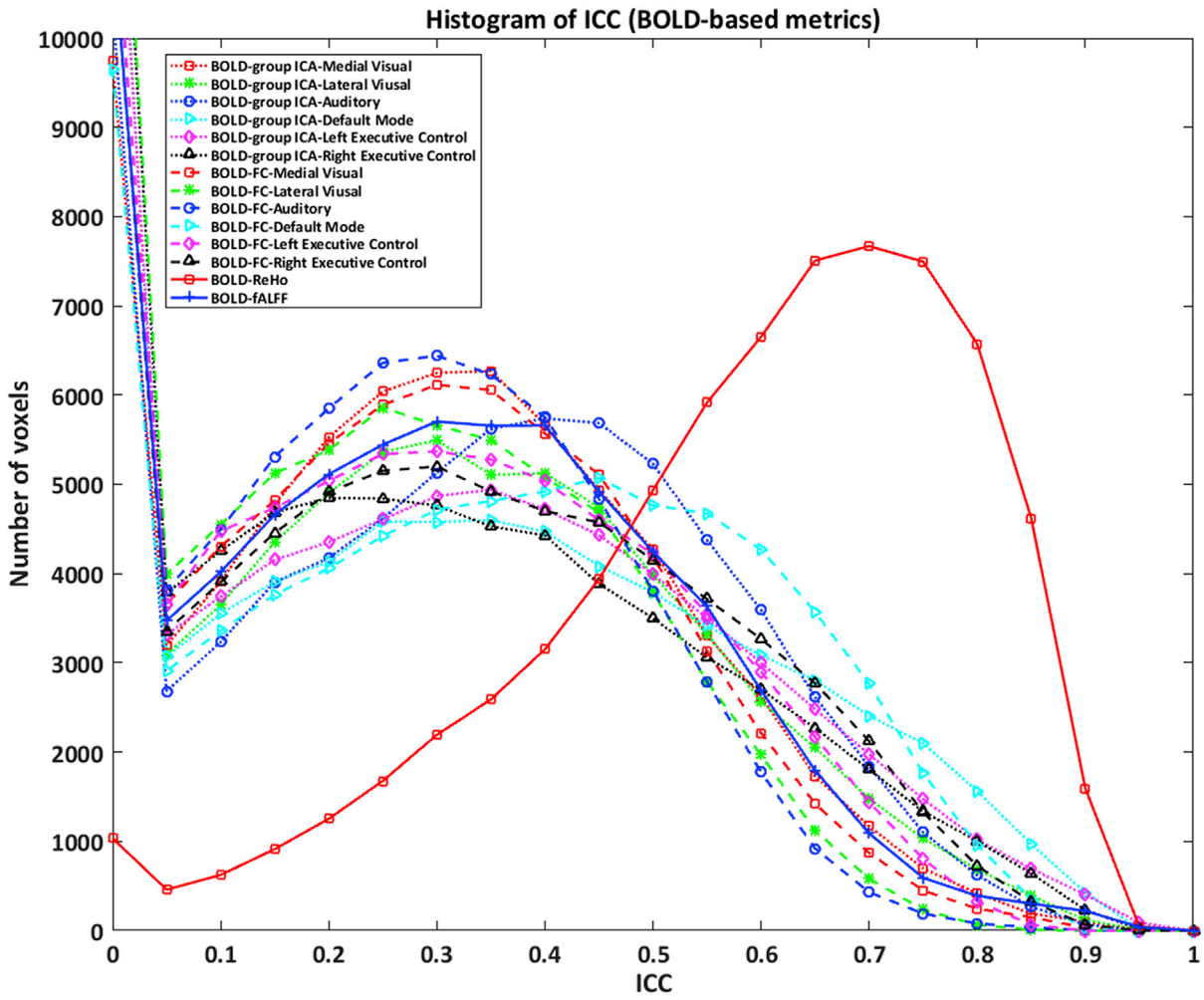

Fig. 10. Histograms of ICC among different BOLD-based indices. The dotted lines indicate the six group ICA networks, the medial visual network, lateral visual network, auditory network, DMN and bilateral ECN. The dashed lines indicate the six FC-based networks. The solid lines indicate the ReHo and fALFF.

on this study's data. The temporal correlation among OEF, R2′, vCBV, and R2 were calculated and showed significant R2′-vCBV, OEF-vCBV and R2′-R2 correlations at the group level (as shown in Fig. S4 in the Supplementary Materials).

Group ICA, seed-based FC, ReHo and fALFF analyses were performed on the OEF-weighted, vCBV-weighted, R2-weighted and R2′-weighted signals separately. Group ICA analyses showed that OEF-weighted and R2′-weighted signals provided robust functional networks, including the medial visual, lateral visual, auditory, default mode and bilateral ECNs (Fig. 13). Only three networks, including the medial visual network, the lateral visual network and the DMN, were identified from the R2-weighted fluctuations, and no physiologically meaningful networks were identified from the vCBV-weighted fluctuations. Seed-based FC analyses showed similar connectivity results for the OEF-weighted, vCBV-weighted, R2-weighted and R2′-weighted signals (Fig. 14). The R2′-based and vCBV-based results showed that the PCC, MPFC, bilateral angular gyrus, bilateral precuneus and bilateral cuneus had high ReHo (Fig. 15) and high fALFF (Fig. 16) values compared to the whole-brain average values. Similar to the OEF-fALFF results, in addition to the DMN regions, the vCBV-based results also showed high ReHo (Fig. 15) and fALFF (Fig. 16) in other gray matter regions, including the superior temporal gyrus, middle temporal gyrus, rolandic operculum, middle frontal gyrus, opercular part of inferior frontal gyrus, triangular part of inferior frontal gyrus, precentral gyrus and postcentral gyrus. The R2-based results showed that mPFC, angular gyrus, middle temporal gyrus, and middle occipital gyrus had high ReHo (Fig. 15), and the bilateral precuneus, angular gyrus and superior parietal lobe showed high fALFF (Fig. 16). Although the group ICA and seed-based FC results of the R2′-weighted fluctuations were similar to those of the OEF-weighted fluctuations, the spatial patterns of R2′-ReHo and R2′-fALFF were different from those of the OEF-based results. The different resting-state activity patterns between the OEF-based and R2′-based or BOLD-based results likely indicate that the MASE method is not a measure of only R2′, and OEF-weighted fluctuations have specific neurophysiological characteristics.

4. Discussion

In the present study, we investigated resting-state brain networks and local characteristics based on OEF-weighted and BOLD fluctuations in the same group of subjects. Whole-brain OEF-weighted signals were obtained through a newly proposed pulse sequence named MASE (Yin et al., 2018) with a temporal resolution of 3 s. Group ICA and seed-based FC analyses were performed to detect brain networks. ReHo (Zang et al., 2004) and fALFF (Zou et al., 2008) analyses were performed to investigate characteristics of local brain activity. Moreover, the test-retest reliability of the connectivity and local activity based on OEF and BOLD contrasts was further assessed.

Resting-state fMRI studies have significantly improved our understanding of brain activity. Due to its high sensitivity, BOLD contrast has been widely used in resting-state fMRI studies in both health and disease (Biswal et al., 2010; Fox and Raichle, 2007; Zhang and Raichle, 2010).

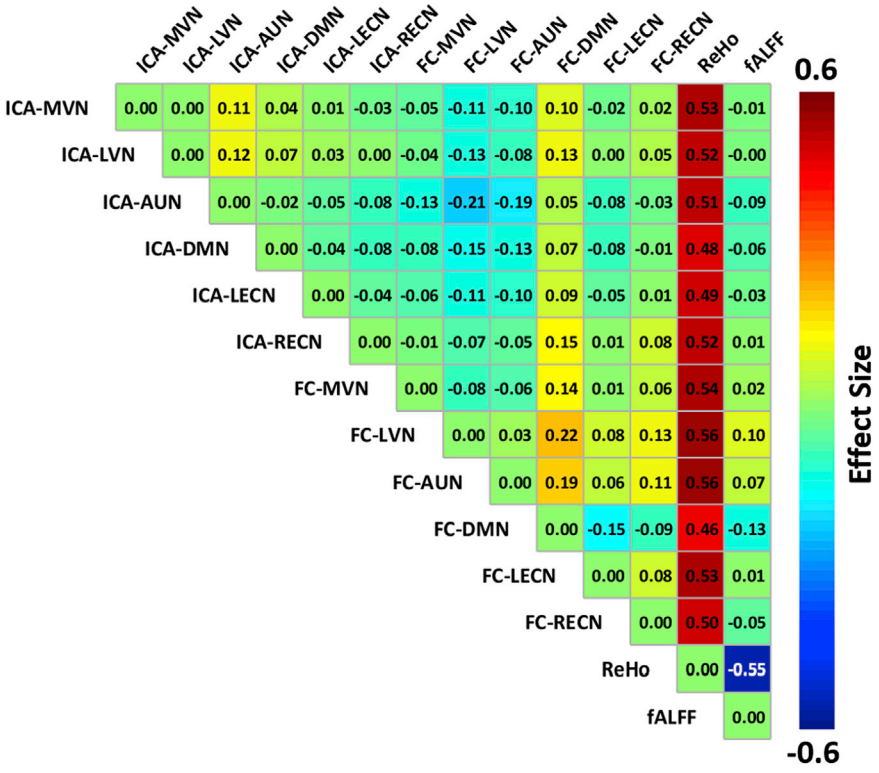

Fig. 11. Effect size of comparisons of ICC histograms between different BOLD-based indices. "MVN", "LVN", "AUN", "DMN", "LECN" and "RECN" indicate the medial visual network, lateral visual network, auditory network, default mode network, left ECN and right ECN, respectively. A positive number shown in a small square indicates that the index above this square exhibits a trend of higher reliability than the index to the left of that square, and a negative number represents the opposite effect.

Table 1
Effect size comparisons of the ICC between the OEF and BOLD contrasts.

Imaging indices	Effect size
ICA-MVN	−0.20
ICA-LVN	−0.20
ICA-AUN	−0.24
ICA-DMN	−0.19
ICA-LECN	−0.21
ICA-RECN	−0.22
FC-MVN	−0.27
FC-LVN	−0.10
FC-AUN	−0.34
FC-DMN	−0.26
FC-LECN	−0.29
FC-RECN	−0.30
ReHo	0.14
fALFF	−0.03

Effect size was calculated from Wilcoxon's signed-rank test (see Eq. (2)). A positive effect size indicates that the corresponding index of OEF contrast had a trend of higher reliability than BOLD, and a negative effect size indicates the opposite.

However, BOLD signal changes depend on the interplay of multiple physiological parameters (Croal et al., 2017; Merola et al., 2017), and BOLD findings are not straightforward to interpret. As such, imaging methods based on a single physiological parameter (such as OEF and $CMRO_2$) are needed to overcome the drawbacks of BOLD contrast. As oxidative metabolism is the primary way in which energy is supplied for human brain activity, abnormal energy demand and metabolism may cause abnormal changes in OEF signals. Previous studies have found that the OEF is closely related to disease activity and might predict an increased risk of stroke in patients with carotid stenosis or occlusion (Gupta et al., 2014), systemic lupus erythematosus (Miyata et al., 2018) and moyamoya disease (Watchmaker et al., 2016). Investigating resting-state brain networks and local activity based on OEF-weighted signals can provide information on brain activity at the oxygen consumption level; moreover, these studies may help in the search for potential biomarkers for the prediction, diagnosis and treatment evaluation of brain diseases.

Largely similar to BOLD, group ICA analysis of OEF-weighted fluctuations revealed prominent resting-state brain networks, including the medial visual network, lateral visual network, auditory network, DMN and bilateral ECN. Not surprisingly, discrepancies between the network patterns obtained from the OEF-weighted and BOLD fluctuations were also present. The brain regions belonging to the OEF-based networks are mostly located in the gray matter, whereas the brain regions belonging to the BOLD networks tend to spread to the white matter. The percentage of the number of voxels in the gray matter was higher in the ICA results for the OEF-based group than in the results for the BOLD group, which could be because the BOLD contrast depends on both intravascular and extravascular effects. In addition, the OEF contrast is mainly derived from the extravascular contribution (Yablonskiy and Haacke, 1994) due to the low blood volume fraction in the parenchyma. At 3T, approximately 33% of the BOLD signal originated intravascularly (Lu and Van Zijl, 2005). A functional motor experiment also demonstrated that the OEF-based activation maps were more localized to the gray matter than the BOLD maps (Yin et al., 2018). Similar to OEF, the CBF and CBV contrasts also showed better spatial localization than BOLD (Duong et al., 2001; Jin and Kim, 2008; Miao et al., 2014). The cerebellum network is a very important brain network that is associated with action and somesthesis (Laird et al., 2011). The lateral visual network spilled into the cerebellum for both the OEF-based and BOLD-based group ICA results, which may be explained in terms of the following aspects. First, the partial volume effect due to the relatively large voxel size during data acquisition, and spatial normalization and smoothing during preprocessing probably blurred the functional signals between the spatially neighboring lateral visual network and cerebellar network. Second, it has also been frequently reported in previous studies that the lateral visual network spills into the cerebellum (see Fig. S5 in the Supplementary Materials) (Beckmann et al., 2005; Calhoun and Adali, 2012; Smith et al., 2009).

To further validate the group ICA findings, we also detected OEF- and BOLD-based networks using a seed-based FC method. In resting-state

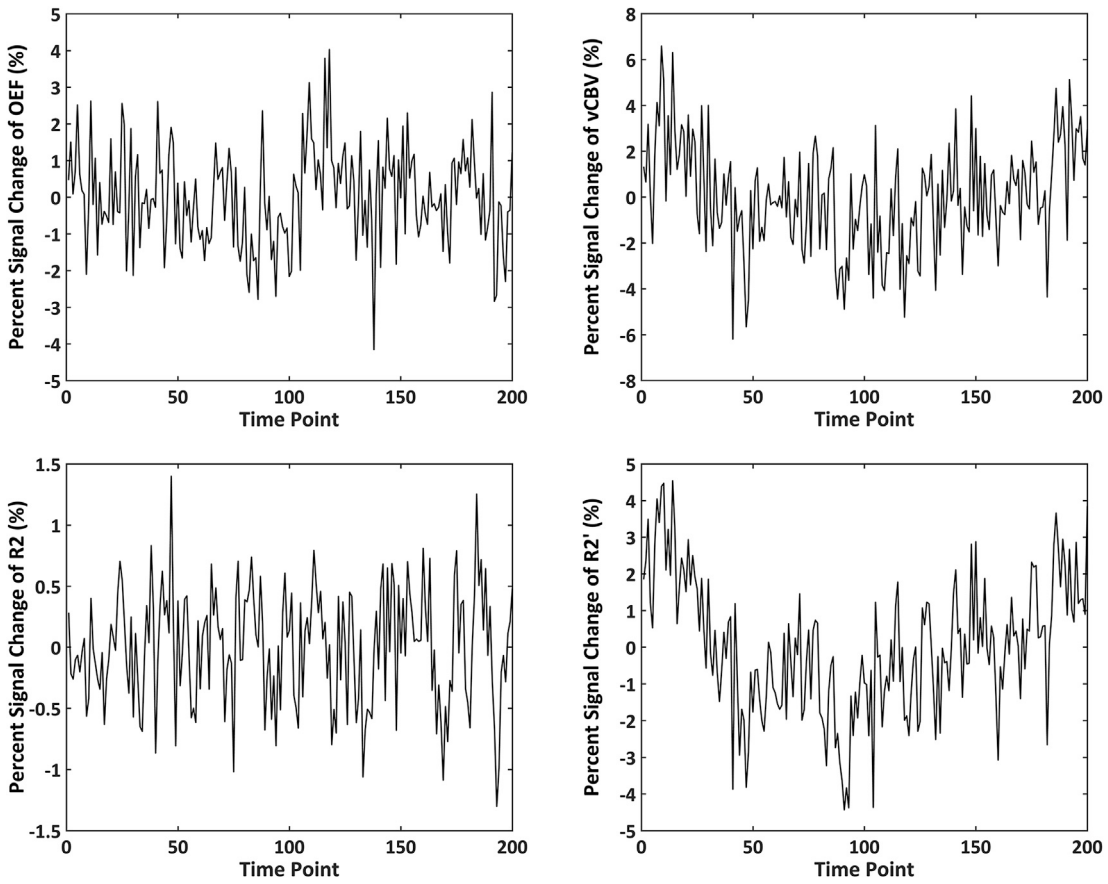

Fig. 12. The time course of the estimated OEF, vCBV, R2 and R2′ from a typical subject in the visual cortex. After motion correction, coregistration, spatial normalization, spatial smoothing (FWHM = 6 mm) and linear detrending of the raw data, the percent signal changes in the visual cortex (sphere centered at (37, −85, 13), with a 10 mm diameter) were calculated.

BOLD fMRI studies (Biswal et al., 2010; Liu et al., 2018; Tang et al., 2018), WM and CSF signals are always regressed out during data preprocessing before seed-based FC analysis. Furthermore, WM and CSF signals are also regressed out in CBF-based (Zou et al., 2015), CBV-based (Miao et al., 2014) and $CMRO_2$-based (Wu et al., 2009a,b) resting-state studies because WM and CSF fluctuations are always classified as non-neuronal noise. FC analysis is used to detect the correlations of different time series obtained from different brain regions. Thus, the correlation of WM or CSF between brain regions could affect the FC results by introducing artifacts. Similar to the analysis of CBF-based, CBV-based and $CMRO_2$-based data, which are also contrasts related to a single physiological mechanism, the WM and CSF signals of OEF-weighted data were regressed out before performing seed-based FC analysis. Similarly, the seed-based FC results of OEF contrast showed better localization in the gray matter than the results of BOLD contrast. It should be noted that the group ICA-generated ECN has two strong lateralized components consisting of parietal and frontal regions for both the OEF and BOLD contrasts, similar to previous BOLD, CBF and CBV findings (Liang et al., 2012; Miao et al., 2014). However, the seed-based ECN maps of BOLD showed stronger connections to the bilateral parietal and frontal regions, and the OEF-based results showed strong bilateral connections in parietal regions and ipsilateral frontal connections. Similarly, seed-based ECN based on CBV showed a strong connection to the bilateral frontal and parietal regions rather than the ipsilateral connection (Miao et al., 2014). Nevertheless, it was not an indication of asymmetry of ECN in the OEF-FC maps. We adopted the laterality index (LI) to quantify the functional asymmetry or laterality (Liu et al., 2009):

$$Laterality\ Index = ((LL - RL) - (RR - LR))/(|LL| + |LR| + |RR| + |RL|) \quad (3)$$

where LL is the strength of the functional connectivity between the left hemisphere seed and the left hemisphere target region; LR represents the strength of the functional connectivity between the left hemisphere seed and right hemisphere target region; and RR and RL represent the contralateral homologues (Liu et al., 2009). Four ROIs (10 mm in diameter) were defined in ECN as follows (Gao and Lin, 2012): the left anterior inferior parietal lobule (−52, −49, 47), the right anterior inferior parietal lobule (52, −46, 46), the left dorsal lateral prefrontal cortex (−50, 20, 34), and the right dorsal lateral prefrontal cortex (46, 14, 43). A low laterality index (−0.04 vs. 0.08) in the ECN for both OEF- and BOLD-weighted fluctuations was observed, which suggested that ECN were symmetric. The missing of contralateral frontal connection in the OEF-FC maps of ECN may be due to relatively low temporal SNR (the ratio of the mean signal to the temporal standard deviation), which was substantially lower than that in the BOLD fluctuations (24 ± 3 versus 203 ± 36).

In this study, we regressed out the six head motion parameters, WM and CSF from the OEF-weighted time series before performing seed-based FC analysis. We recalculated the seed-based FC using the OEF-weighted signals with two other regression strategies. One regressed out the six head motion parameters and CSF signals; the other only regressed out the six head motion parameters. For positive correlations, the results showed almost identical network patterns among the three regression methods (see Fig. S6 in the Supplementary Materials, the maps shown were thresholded at a voxel-level FWE correction of $p < 0.005$).

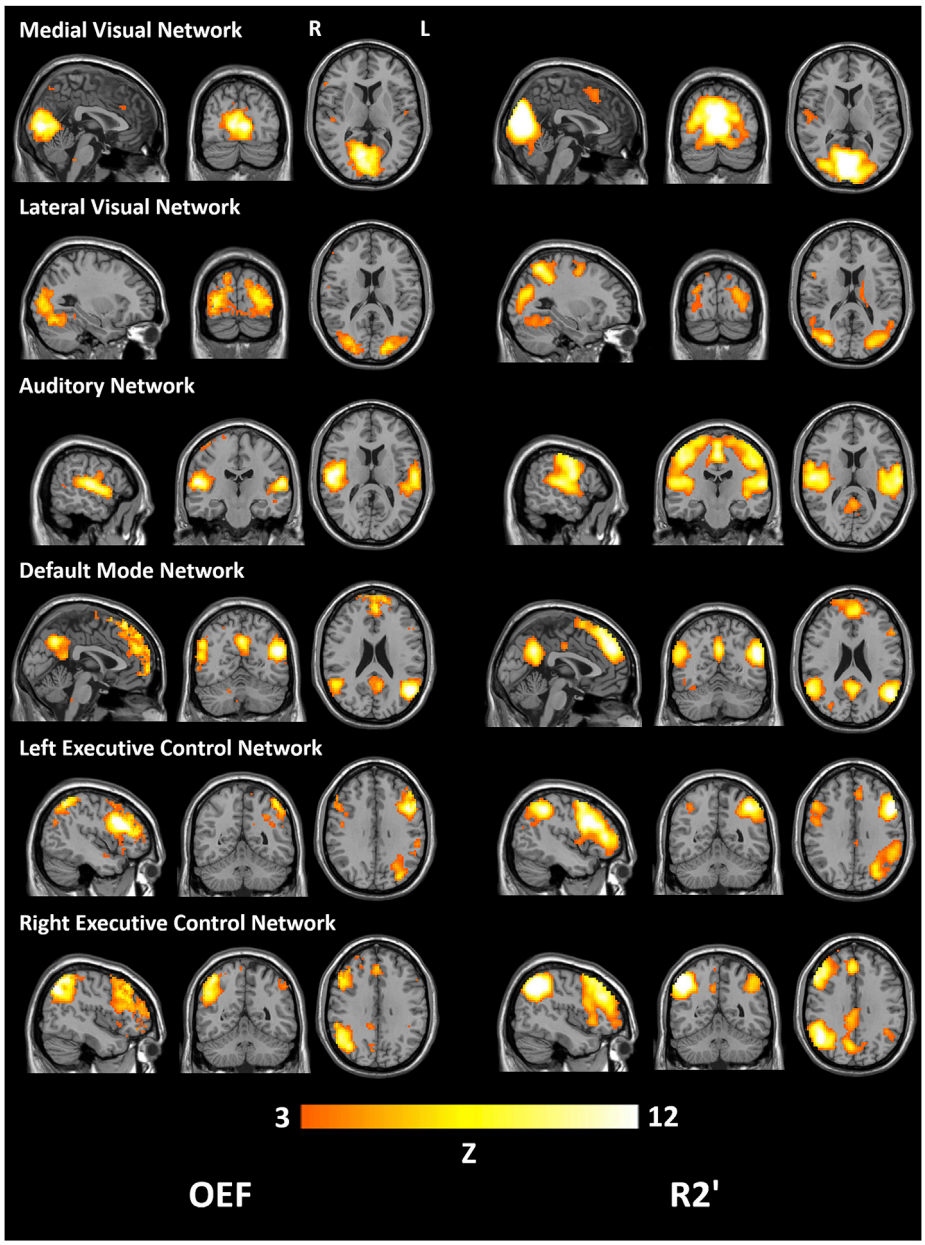

Fig. 13. Functional networks of interest from group ICA of 20 subjects based on the OEF-weighted and R2′-weighted signals from the first scan. The medial visual, lateral visual, auditory, default mode and bilateral executive control networks were identified from 25 components for all of the four contrasts. All ICA spatial maps were converted to Z statistic maps via a mixture-model fit and thresholded at $Z > 3$.

For anti correlations, after voxel-level correction of $p < 0.01$ (no significant anti correlations remained with threshold setting at a voxel-level FWE correction of $p < 0.005$), the results showed minor differences in the gray matter among the three regression methods (see Fig. S7 in the Supplementary Materials). It should be noted that differences mainly occurred at WM and CSF regions, and the more variances of non-interest were regressed out, the more anti-correlated voxels were observed (6344 voxels for head motion + CSF + WM, 2685 voxels for head motion + CSF, and 2569 voxels for head motion only).

In addition to investigations of brain networks, we further explored local brain activity based on OEF-weighted fluctuations using two different methods: ReHo and fALFF. ReHo (Zang et al., 2004) was used to detect the local synchrony specificity of signals by measuring the similarity of the time courses of the voxels within a given cluster. Several previous studies have demonstrated that ReHo can be a useful tool to reveal the pathophysiology underlying brain diseases, such as Parkinson's disease (Wu et al., 2009a,b), depression (Guo et al., 2011; Liu et al., 2010) and autism spectrum disorders (Paakki et al., 2010). Similar to previous BOLD and CBF (Zou et al., 2009) studies, high ReHo of both OEF-weighted and BOLD fluctuations in this study was shown in the PCC, MPFC, bilateral angular gyrus, bilateral precuneus and bilateral cuneus. The PCC and MPFC showed high ReHo in both the OEF-based and BOLD-based results. However, the t-value of PCC in the OEF-ReHo maps was smaller than that of MPFC, which is different from BOLD in that the local synchrony of PCC was higher than the MPFC in the BOLD results. This difference might be due to the specific characteristics of the similarity of the OEF-weighted time courses. The gradient-echo EPI sequence used in the present study is sensitive to susceptibility artifacts at the interfaces of brain tissue and air/bone, which may cause spatial distortion and signal loss, especially in the orbitofrontal cortex. The medial prefrontal area is located near the orbitofrontal cortex, which might explain the low BOLD-ReHo value in the medial frontal area, while the MASE

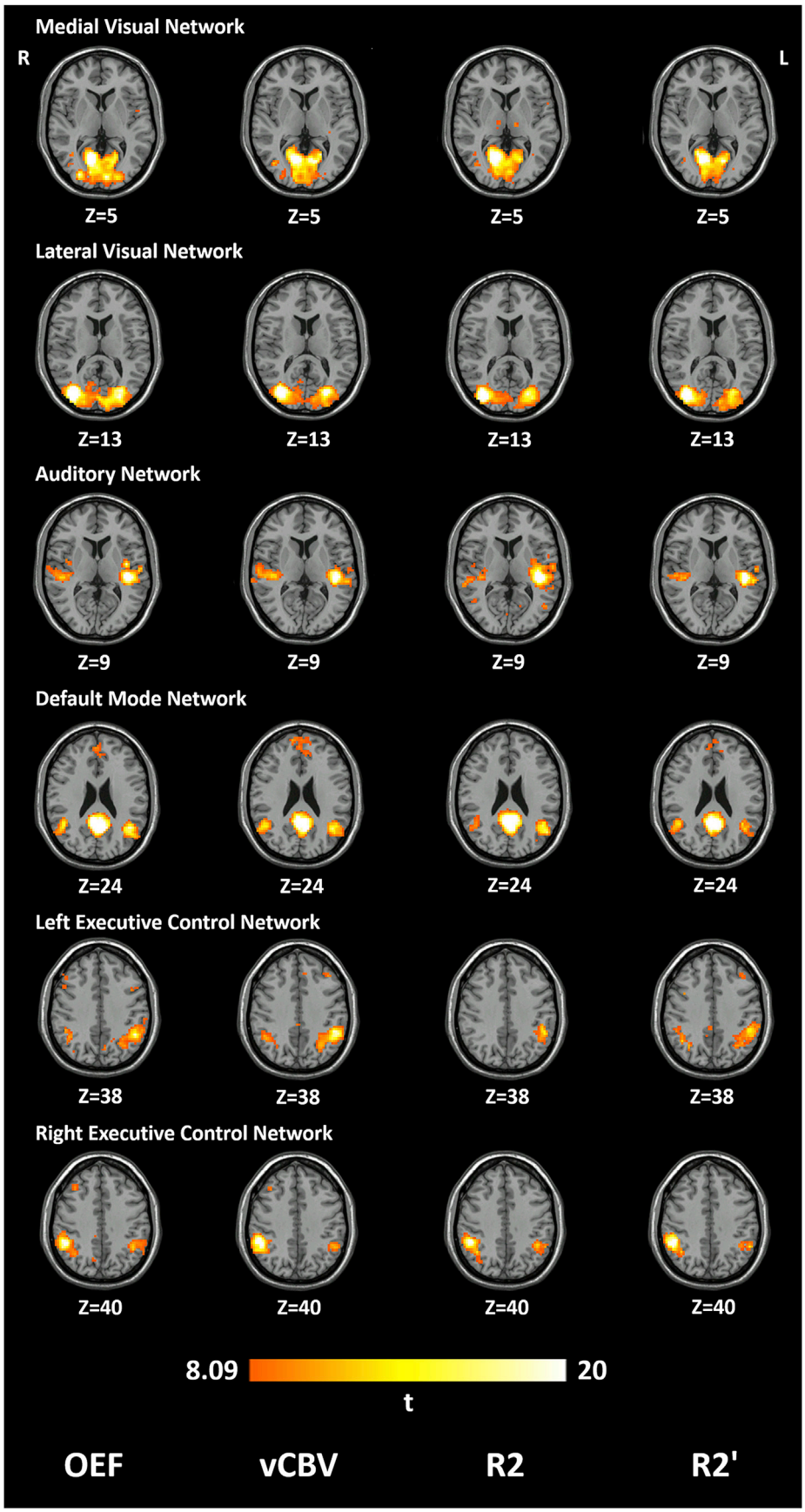

Fig. 14. Seed-based FC maps of 20 subjects based on the OEF-weighted, vCBV-weighted, R2-weighted and R2′-weighted signals from the first scan. The numbers below the maps are Z coordinates in the axial view in MNI space. These networks include the medial visual, lateral visual, auditory, default mode and bilateral executive control networks. The connectivity maps were thresholded at voxel-level FWE correction of $p < 0.005$.

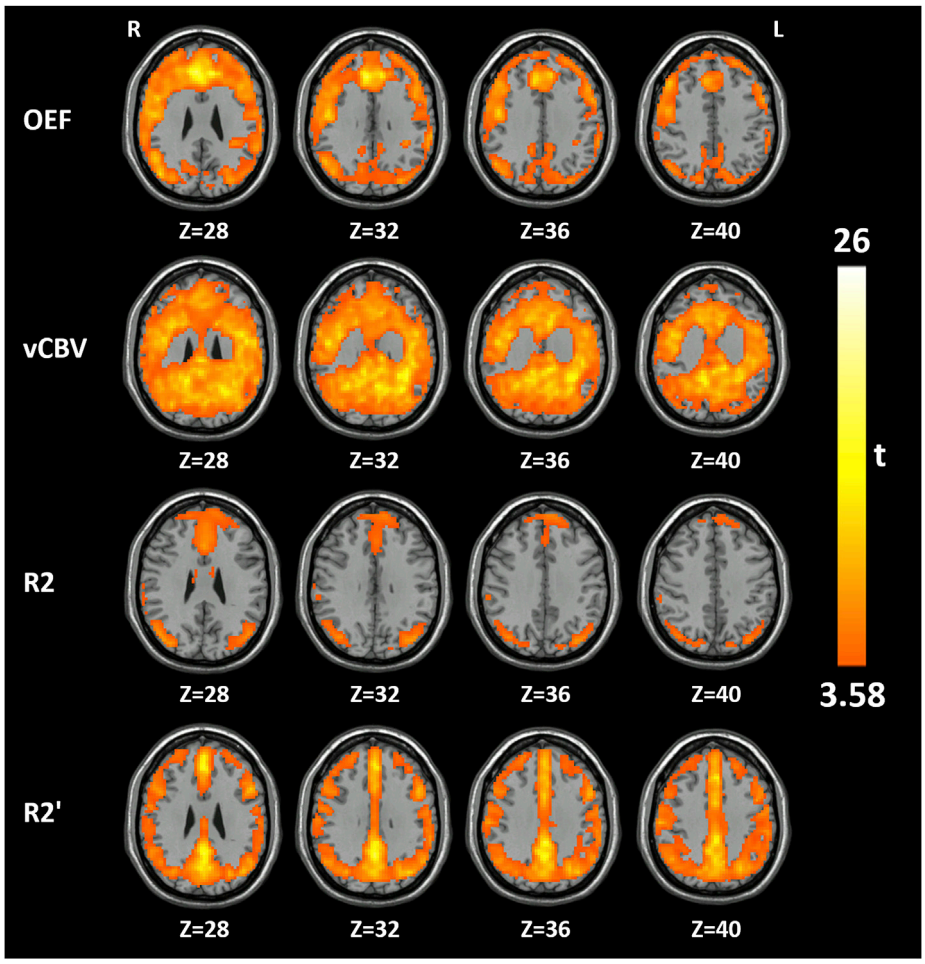

Fig. 15. ReHo maps of 20 subjects based on the OEF-weighted, vCBV-weighted, R2-weighted and R2′-weighted signals from the first scan. The numbers below the maps are Z coordinates in the axial view in MNI space. The results from a one-sample *t*-test on the ReHo maps were thresholded at voxel-level $p < 0.001$ with a cluster-level FDR correction of $p < 0.05$.

sequence signals were acquired after a 180° refocusing pulse, which can diminish the spatial distortion and signal loss effects to some extent. Moreover, the OEF-weighted time courses might occur at a different timescale compared with BOLD fluctuations. The above ReHo results were calculated from filtered (0.01–0.08 Hz) OEF-weighted data. Bandpass filtering is usually used to eliminate the effects of physiological noise in BOLD-related resting-state studies. In the present study, we performed bandpass filtering on OEF-weighted fluctuations, consistent with that of BOLD analysis. Additional OEF-ReHo results based on unfiltered data showed improvement of the ReHo strength in the PCC, which suggested that higher-frequency (>0.1 Hz) OEF-weighted fluctuations contributed to the ReHo measurement, especially for the PCC region (see Fig. S8 in the Supplementary Materials for the comparison of OEF-ReHo results based on filtered and unfiltered data). The mechanisms underlying the higher-frequency (>0.1 Hz) OEF-weighted fluctuations are unknown and need to be further investigated. The local activity amplitude characteristics were detected using fALFF (Zou et al., 2008), which has been widely applied to brain diseases, such as schizophrenia (Hoptman et al., 2010; Yu et al., 2014), amnestic mild cognitive impairment (Han et al., 2011) and migraine (Wang et al., 2016). The fALFF results of BOLD signals showed that the PCC, MPFC, bilateral middle frontal gyrus, angular gyrus, precuneus and cuneus had significantly higher fALFF values than the whole-brain average, which was similar to the results of a previous study (Zou et al., 2008). Additional brain regions belonging to the auditory network, the sensorimotor network and certain cerebellar regions also showed higher fALFF values than the whole-brain average for OEF-fALFF, which indicates that the ratio of the power in the low-frequency range to that of the entire frequency range of these brain regions was similar but still different in certain white matter regions for OEF contrast. These results differed from the BOLD-fALFF results, which was likely due to the different frequency characteristics of OEF-weighted fluctuations. Similarly, the CBV-weighted time course shows more high-frequency oscillations (Miao et al., 2014) than BOLD. The neurophysiological mechanisms that underlie the higher fALFF values across almost the whole gray matter in the cerebral cortex warrants further investigation, possibly through simultaneous EEG-OEF fMRI studies that relate the frequency characteristics of OEF-weighted fluctuations to electrophysiology.

The third or fourth echo data acquired in the MASE sequence could be used as BOLD contrast. We calculated group ICA, seed-based FC, ReHo and fALFF using the third echo (TE = 80 ms) of MASE. The preprocessing procedures of the third echo data were same with BOLD-based procedures as described above. The results were similar to the BOLD results. Six resting functional networks, the medial visual network, the lateral visual network, the auditory network, the DMN, and the left and right ECN, were identified as biologically meaningful out of the 25 components generated by group ICA (see Fig. S9 in the Supplementary Materials). Similar network maps were produced through seed-based FC analysis (see Fig. S10 in the Supplementary Materials). The PCC, MPFC, bilateral angular gyrus, bilateral precuneus and bilateral cuneus showed high ReHo (see Fig. S11 in the Supplementary Materials) and high fALFF values (see Fig. S11 in the Supplementary Materials) compared to the

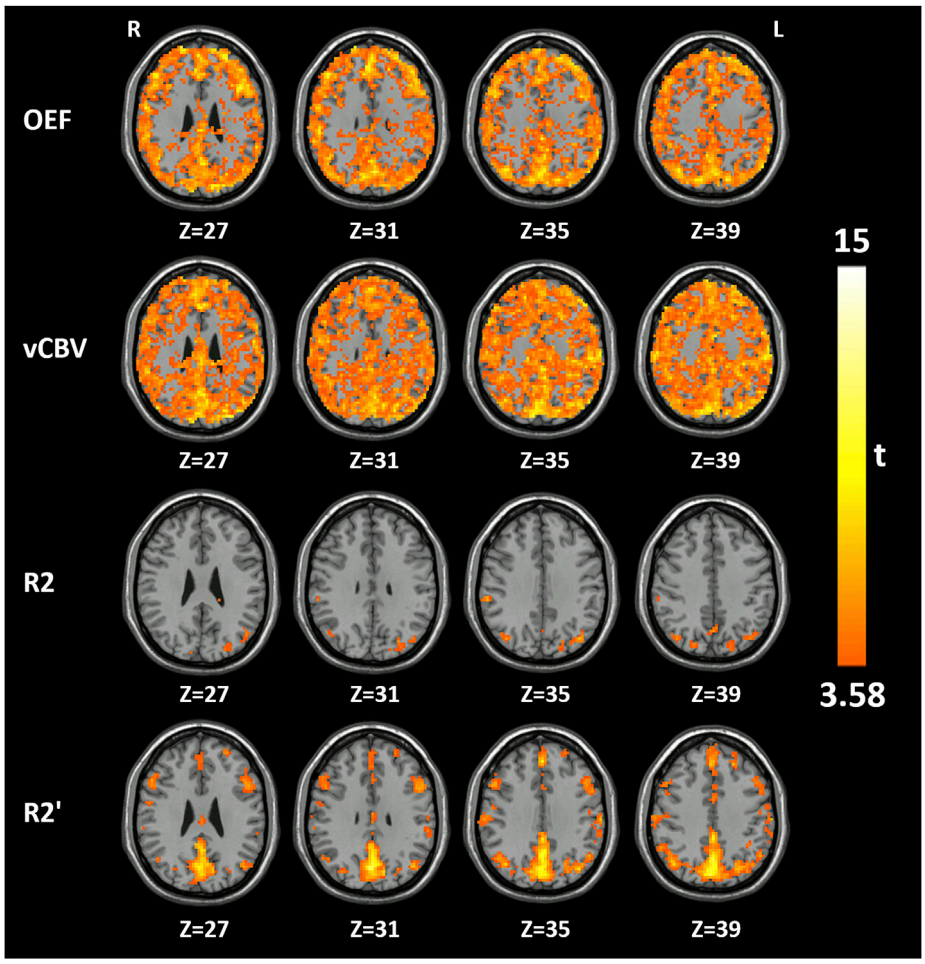

Fig. 16. fALFF maps of 20 subjects based on the OEF-weighted, vCBV-weighted, R2-weighted and R2′-weighted signals from the first scan. The numbers below the maps are Z coordinates in the axial view in MNI space. The results from a one-sample *t*-test on the fALFF maps were thresholded at voxel-level $p < 0.001$ with a cluster-level FDR correction of $p < 0.05$.

whole-brain average. These results suggested that MASE could provide BOLD contrast, thus avoiding separate BOLD fMRI acquisition in future studies.

Evaluating the test-retest reliability of brain activity measurements has crucial importance (Jahng et al., 2005; Jann et al., 2015a; Patriat et al., 2013a; Zhu et al., 2014). Comparisons between the ICC histograms of connectivity and local characteristics indices based on the OEF contrast showed that OEF-ReHo had the highest reliability, and OEF-fALFF had a higher reliability than all network indices, including the six group ICA components and six seed-based FC maps. Notably, the ICC histogram of OEF-fALFF had a second peak of approximately 0.9 (Fig. 6), which was different from the other OEF-based indices and all BOLD-based indices. The regions with extremely high ICC (>0.8) were located near the ventricles and large blood vessels and might be due mainly to noise fluctuations. Nevertheless, comparisons of the ICC histograms lower than 0.8 still showed that OEF-fALFF also had a trend of higher reliability than any of the network indices with minimal to small effect sizes, except for the FC-based DMN (see Fig. S12 in the Supplementary Materials). The physiological noise effects can be highly reliable. As demonstrated in our previous study, physiological noise, such as respiration and cardiac fluctuations, increased the reliability of both BOLD and CBF functional activities (Zou et al., 2015). Although we have made efforts to eliminate physiological contaminants by regressing out the fluctuations of the CSF and white matter, the brain regions with high ICC extended to the white matter for both OEF-ReHo and BOLD-ReHo, as shown in Fig. 8.

Comparison of the ICC of the different metrics between OEF and BOLD contrasts showed that OEF-ReHo had higher reliability than BOLD-ReHo, although the effect size was small. Except for ReHo, all the other metrics based on OEF-weighted fluctuations had lower reliability than BOLD, with small to medium effect sizes. The OEF-based ICC scores were generally lower than the BOLD-based scores, which is likely driven by the relatively low SNR of OEF-weighted signals. The comparison of the reliability of spontaneous brain activities between the CBF and BOLD contrasts suggested that CBF-FC and CBF-ALFF had lower reliability than BOLD-FC and BOLD-ALFF, respectively, which could be due to the low SNR of CBF signals (Zou et al., 2015). Both OEF and CBF are important single physiological parameters; the reliability results of OEF contrast in the present study were consistent with the CBF-related studies (Zou et al., 2015). Furthermore, these differences in ICC may arise from differences in sensitivity and the physiological mechanism between OEF and BOLD contrasts. High sensitivity is generally observed for BOLD, which yields relatively high ICC for the BOLD contrast. On the other hand, OEF is a single physiological parameter, which can reflect the amount of oxygen that leaves the blood stream to enter the surrounding tissues, while BOLD signal changes depend on the interplay of multiple physiological parameters, which might account for the high ICC for OEF-ReHo but warrant further investigation. These results suggest that in terms of test-retest reliability, the OEF-ReHo index is even better than BOLD for the purpose of investigating local synchrony of resting-state brain activity.

We adopted the ICC as a measurement of reliability in the current

study. The ICC calculation adopted in this study does not penalize for systematic errors, such as the differences in brain activity between scans (Zuo et al., 2010c). Its usage is recommended for test-retest situations in which systematic errors due to learning effects or fatigue effects may occur, which are not directly related to reliability (Rousson et al., 2002; Weir, 2005). Although the ICC has been widely used in neuroimaging studies (Andellini et al., 2015; Hodkinson et al., 2013b; Jann et al., 2015b; Patriat et al., 2013b; Zou et al., 2015), there are still some other measures we can use to detect the test-retest reliability including Bland-Altman plots, the coefficient of variation and the Pearson r (Weir, 2005). A methodology investigation on the comparison of different metrics for test-retest reliability analyses is warranted in the near future.

Some questions should be investigated in future studies. First, the partial volume effects of cerebrospinal fluid (CSF) would result in an overestimation of OEF (Stone and Blockley, 2017), and the influence of CSF signals on OEF-weighted signals could partly account for the noise in OEF-weighted images. To reduce the CSF effect, Stone and Blockley (2017) used a fluid-attenuated inversion recovery (FLAIR) preparation to suppress CSF signals during data acquisition. VASO-related studies (Miao et al., 2014) also indicated that the influence of CSF signals on VASO signals could partly account for the noise in VASO images, and VASO-FLAIR could nullify the CSF signal in VASO imaging to improve image quality. Similarly, FLAIR can be implemented together with MASE to attenuate the effect of CSF signals on dynamic measurement of the OEF-weighted signals. Second, the origins of OEF changes are related to CBF fluctuations, and both CBF and OEF-weighted fluctuations are related to neuronal activity (Biswal et al., 1997; Chuang et al., 2008; Yin et al., 2018). Spontaneous CBF fluctuations reflect changes in blood flow (Zou et al., 2009), while OEF-weighted fluctuations can reflect changes in oxygen consumption (Stout et al., 2018). The relationship between CBF changes and oxygen consumption is not fully understood yet and needs further investigation in future studies. Third, OEF has an explicit physiological meaning, and OEF-based brain activity investigations could more directly reveal the basic mechanisms of brain activity. Previous studies have found that the OEF is closely related to dysfunction in patients with brain diseases (Gupta et al., 2014; Miyata et al., 2018; Watchmaker et al., 2016), but no study has investigated the underlying pathophysiological mechanisms underlying brain diseases through dynamic OEF-weighted fluctuations. In future studies, the difference in brain activity between normal subjects and patients can be detected using OEF-weighted fluctuations based on the MASE sequence. Fourth, PET is a standard method for quantitatively measuring OEF. We will compare the OEF values measured by the MASE sequence, with PET results to test if the MASE sequence can truly measure OEF in the future. Finally, the specific frequency characteristics of OEF-weighted fluctuations were not systematically investigated in this study. The neurophysiological mechanisms that underlie the higher-frequency OEF-weighted fluctuations need further investigation. Simultaneous EEG-BOLD fMRI has been proven useful for investigating the relationship between hemodynamic fluctuations and electrophysiological oscillations (Laufs et al., 2003; Mantini et al., 2007). Simultaneous EEG-OEF fMRI could be used in further studies to investigate the relationship between the frequency characteristics of OEF-weighted signals and electrophysiology.

5. Conclusions

In the present study, we demonstrated that intrinsic brain activity could be detected by spontaneous fluctuations of OEF-weighted signals using a MASE imaging technique. The relatively high temporal resolution of MASE makes it possible to acquire whole-brain OEF-weighted images within 3 s. To our knowledge, this study is the first investigation of OEF-based brain networks and local dynamic brain activity of the whole brain in the resting state. Consistent with the BOLD findings, several reliable resting-state brain networks were detected from the OEF-weighted voxel-wise fluctuations, including the medial visual network, lateral visual network, auditory network, DMN, and left and right ECN. The PCC, MPFC, bilateral angular gyrus, bilateral precuneus and bilateral cuneus showed higher ReHo and fALFF values based on OEF-weighted fluctuations. Test-retest reliability results showed that OEF-ReHo had slightly higher ICC than BOLD, although the ICC of other resting-state brain activity indices was generally lower based on OEF-weighted fluctuations than based on BOLD. In conclusion, OEF can be used as an effective contrast to investigate resting-state brain networks and local dynamic characteristics.

6. Declarations of interest

None.

Acknowledgements

This work was supported by National Key Research and Development Program of China (grant numbers 2018YFC2000603 and 2017YFC0108900); the China's National Strategic Basic Research Program (“973”) (grant number 2015CB856400); the National Natural Science Foundation of China (grant numbers 81871427, 81671765, 81430037, 81727808, 81790650, 81790651, 31421003, and 81522021); the Beijing Municipal Natural Science Foundation (grant number 7172121); the Beijing Municipal Science and Technology Commission (grant numbers Z181100001518005, Z161100002616006, and Z171100000117012); the Shenzhen Peacock Plan (grant number KQTD2015033016104926); the Guangdong Pearl River Talents Plan Innovative and Entrepreneurial Team (grant number 2016ZT06S220); and the Shenzhen Science and Technology Research Funding Program (grant number JCYJ20170412164413575). We thank the National Center for Protein Sciences at Peking University in Beijing, China, for assistance with the MRI data acquisition and data analyses.

Appendix A. Supplementary data

Supplementary data to this article can be found online at https://doi.org/10.1016/j.neuroimage.2019.06.038.

References

Andellini, M., Cannatà, V., Gazzellini, S., Bernardi, B., Napolitano, A., 2015. Test-retest reliability of graph metrics of resting state MRI functional brain networks: a review. J. Neurosci. Methods 253, 183–192. https://doi.org/10.1016/j.jneumeth.2015.05.020.

Beckmann, C.F., DeLuca, M., Devlin, J.T., Smith, S.M., 2005. Investigations into resting-state connectivity using independent component analysis. Philos. Trans. R. Soc. Lond. B Biol. Sci. 360, 1001–1013. https://doi.org/10.1098/rstb.2005.1634.

Biswal, B.B., Kylen, J.V., Hyde, J.S., 1997. Simultaneous assessment of flow and BOLD signals in resting-state functional connectivity maps. NMR Biomed. 10, 165–170.

Biswal, B.B., Mennes, M., Zuo, X.-N., Gohel, S., Kelly, C., Smith, S.M., Beckmann, C.F., Adelstein, J.S., Buckner, R.L., Colcombe, S., Dogonowski, A.-M., Ernst, M., Fair, D., Hampson, M., Hoptman, M.J., Hyde, J.S., Kiviniemi, V.J., Kötter, R., Li, S.-J., Lin, C.-P., Lowe, M.J., Mackay, C., Madden, D.J., Madsen, K.H., Margulies, D.S., Mayberg, H.S., McMahon, K., Monk, C.S., Mostofsky, S.H., Nagel, B.J., Pekar, J.J., Peltier, S.J., Petersen, S.E., Riedl, V., Rombouts, S.A.R.B., Rypma, B., Schlaggar, B.L., Schmidt, S., Seidler, R.D., Siegle, G.J., Sorg, C., Teng, G.-J., Veijola, J., Villringer, A., Walter, M., Wang, L., Weng, X.-C., Whitfield-Gabrieli, S., Williamson, P., Windischberger, C., Zang, Y.-F., Zhang, H.-Y., Castellanos, F.X., Milham, M.P., 2010. Toward discovery science of human brain function. Proc. Natl. Acad. Sci. Unit. States Am. 107, 4734–4739. https://doi.org/10.1073/pnas.0911855107.

Bush, A.M., Coates, T.D., Wood, J.C., 2018. Diminished cerebral oxygen extraction and metabolic rate in sickle cell disease using T2 relaxation under spin tagging MRI. Magn. Reson. Med. 80, 294–303. https://doi.org/10.1002/mrm.27015.

Calhoun, V.D., Adali, T., 2012. Multisubject independent component analysis of fMRI: a decade of intrinsic networks, default mode, and neurodiagnostic discovery. IEEE Rev. Biomed. Eng. 5, 60–73. https://doi.org/10.1109/RBME.2012.2211076.

Chuang, K.-H., van Gelderen, P., Merkle, H., Bodurka, J., Ikonomidou, V.N., Koretsky, A.P., Duyn, J.H., Talagala, S.L., 2008. Mapping resting-state functional connectivity using perfusion MRI. Neuroimage 40, 1595–1605. https://doi.org/10.1016/j.neuroimage.2008.01.006.

Croal, P.L., Driver, I.D., Francis, S.T., Gowland, P.A., 2017. Field strength dependence of grey matter R2* on venous oxygenation. Neuroimage 146, 327–332. https://doi.org/10.1016/j.neuroimage.2016.10.004.

Damoiseaux, J.S., Rombouts, S. a. R.B., Barkhof, F., Scheltens, P., Stam, C.J., Smith, S.M., Beckmann, C.F., 2006. Consistent resting-state networks across healthy subjects.

Proc. Natl. Acad. Sci. Unit. States Am. 103, 13848–13853. https://doi.org/10.1073/pnas.0601417103.
Davis, T.L., Kwong, K.K., Weisskoff, R.M., Rosen, B.R., 1998. Calibrated functional MRI: mapping the dynamics of oxidative metabolism. Proc. Natl. Acad. Sci. Unit. States Am. 95, 1834–1839. https://doi.org/10.1073/pnas.95.4.1834.
De Luca, M., Beckmann, C.F., De Stefano, N., Matthews, P.M., Smith, S.M., 2006. fMRI resting state networks define distinct modes of long-distance interactions in the human brain. Neuroimage 29, 1359–1367. https://doi.org/10.1016/j.neuroimage.2005.08.035.
Detre, J.A., Leigh, J.S., Williams, D.S., Koretsky, A.P., 1992. Perfusion imaging. Magn. Reson. Med. 23, 37–45. https://doi.org/10.1002/mrm.1910230106.
Duong, T.Q., Kim, D.-S., Uğurbil, K., Kim, S.-G., 2001. Localized cerebral blood flow response at submillimeter columnar resolution. Proc. Natl. Acad. Sci. Unit. States Am. 98, 10904–10909. https://doi.org/10.1073/pnas.191101098.
Elton, A., Gao, W., 2015. Task-related modulation of functional connectivity variability and its behavioral correlations. Hum. Brain Mapp. 36, 3260–3272. https://doi.org/10.1002/hbm.22847.
Fox, M.D., Raichle, M.E., 2007. Spontaneous fluctuations in brain activity observed with functional magnetic resonance imaging. Nat. Rev. Neurosci. 8, 700–711. https://doi.org/10.1038/nrn2201.
Gao, W., Lin, W., 2012. Frontal parietal control network regulates the anti-correlated default and dorsal attention networks. Hum. Brain Mapp. 33, 192–202. https://doi.org/10.1002/hbm.21204.
Greicius, M.D., Krasnow, B., Reiss, A.L., Menon, V., 2003. Functional connectivity in the resting brain: a network analysis of the default mode hypothesis. Proc. Natl. Acad. Sci. Unit. States Am. 100, 253–258. https://doi.org/10.1073/pnas.0135058100.
Guo, W., Sun, X., Liu, L., Xu, Q., Wu, R., Liu, Z., Tan, C., Chen, H., Zhao, J.-P., 2011. Disrupted regional homogeneity in treatment-resistant depression: a resting-state fMRI study. Prog. Neuro-Psychopharmacol. Biol. Psychiatry 35, 1297–1302. https://doi.org/10.1016/j.pnpbp.2011.02.006.
Gupta, A., Baradaran, H., Schweitzer, A.D., Kamel, H., Pandya, A., Delgado, D., Wright, D., Hurtado-Rua, S., Wang, Y., Sanelli, P.C., 2014. Oxygen extraction fraction and stroke risk in patients with carotid stenosis or occlusion: a systematic review and meta-analysis. Am. J. Neuroradiol. https://doi.org/10.3174/ajnr.A3668.
Han, Y., Wang, J., Zhao, Z., Min, B., Lu, J., Li, K., He, Y., Jia, J., 2011. Frequency-dependent changes in the amplitude of low-frequency fluctuations in amnestic mild cognitive impairment: a resting-state fMRI study. Neuroimage 55, 287–295. https://doi.org/10.1016/j.neuroimage.2010.11.059.
He, X., Yablonskiy, D.A., 2007. Quantitative BOLD: mapping of human cerebral deoxygenated blood volume and oxygen extraction fraction: default state. Magn. Reson. Med. 57, 115–126. https://doi.org/10.1002/mrm.21108.
Heine, L., Soddu, A., Gomez, F., Vanhaudenhuyse, A., Tshibanda, L., Thonnard, M., Charland-Verville, V., Kirsch, M., Laureys, S., Demertzi, A., 2012. Resting state networks and consciousness. Front. Psychol. 3. https://doi.org/10.3389/fpsyg.2012.00295.
Hodkinson, D.J., Krause, K., Khawaja, N., Renton, T.F., Huggins, J.P., Vennart, W., Thacker, M.A., Mehta, M.A., Zelaya, F.O., Williams, S.C.R., Howard, M.A., 2013a. Quantifying the test–retest reliability of cerebral blood flow measurements in a clinical model of on-going post-surgical pain: a study using pseudo-continuous arterial spin labelling. NeuroImage Clin 3, 301–310. https://doi.org/10.1016/j.nicl.2013.09.004.
Hodkinson, D.J., Krause, K., Khawaja, N., Renton, T.F., Huggins, J.P., Vennart, W., Thacker, M.A., Mehta, M.A., Zelaya, F.O., Williams, S.C.R., Howard, M.A., 2013b. Quantifying the test–retest reliability of cerebral blood flow measurements in a clinical model of on-going post-surgical pain: a study using pseudo-continuous arterial spin labelling. NeuroImage Clin 3, 301–310. https://doi.org/10.1016/j.nicl.2013.09.004.
Hoptman, M.J., Zuo, X.-N., Butler, P.D., Javitt, D.C., D'Angelo, D., Mauro, C.J., Milham, M.P., 2010. Amplitude of low-frequency oscillations in schizophrenia: a resting state fMRI study. Schizophr. Res. 117, 13–20. https://doi.org/10.1016/j.schres.2009.09.030.
Hyder, F., Herman, P., Bailey, C.J., Møller, A., Globinsky, R., Fulbright, R.K., Rothman, D.L., Gjedde, A., 2016. Uniform distributions of glucose oxidation and oxygen extraction in gray matter of normal human brain: no evidence of regional differences of aerobic glycolysis. J. Cereb. Blood Flow Metab. 36, 903–916. https://doi.org/10.1177/0271678X15625349.
Jahng, G.-H., Song, E., Zhu, X.-P., Matson, G.B., Weiner, M.W., Schuff, N., 2005. Human brain: reliability and reproducibility of pulsed arterial spin-labeling perfusion MR imaging. Radiology 234, 909–916. https://doi.org/10.1148/radiol.2343031499.
Jann, K., Gee, D.G., Kilroy, E., Schwab, S., Smith, R.X., Cannon, T.D., Wang, D.J.J., 2015a. Functional connectivity in BOLD and CBF data: similarity and reliability of resting brain networks. Neuroimage 106, 111–122. https://doi.org/10.1016/j.neuroimage.2014.11.028.
Jann, K., Gee, D.G., Kilroy, E., Schwab, S., Smith, R.X., Cannon, T.D., Wang, D.J.J., 2015b. Functional connectivity in BOLD and CBF data: similarity and reliability of resting brain networks. Neuroimage 106, 111–122. https://doi.org/10.1016/j.neuroimage.2014.11.028.
Jin, T., Kim, S.-G., 2008. Improved cortical-layer specificity of vascular space occupancy fMRI with slab inversion relative to spin-echo BOLD at 9.4 T. Neuroimage 40, 59–67. https://doi.org/10.1016/j.neuroimage.2007.11.045.
Küblböck, M., Woletz, M., Höflich, A., Sladky, R., Kranz, G.S., Hoffmann, A., Lanzenberger, R., Windischberger, C., 2014. Stability of low-frequency fluctuation amplitudes in prolonged resting-state fMRI. Neuroimage 103, 249–257. https://doi.org/10.1016/j.neuroimage.2014.09.038.
Laird, A.R., Fox, P.M., Eickhoff, S.B., Turner, J.A., Ray, K.L., McKay, D.R., Glahn, D.C., Beckmann, C.F., Smith, S.M., Fox, P.T., 2011. Behavioral interpretations of intrinsic connectivity networks. J. Cogn. Neurosci. 23, 4022–4037. https://doi.org/10.1162/jocn_a_00077.
Laufs, H., Krakow, K., Sterzer, P., Eger, E., Beyerle, A., Salek-Haddadi, A., Kleinschmidt, A., 2003. Electroencephalographic signatures of attentional and cognitive default modes in spontaneous brain activity fluctuations at rest. Proc. Natl. Acad. Sci. Unit. States Am. 100, 11053–11058. https://doi.org/10.1073/pnas.1831638100.
Li, Z., Kadivar, A., Pluta, J., Dunlop, J., Wang, Z., 2012. Test–retest stability analysis of resting brain activity revealed by blood oxygen level-dependent functional MRI. J. Magn. Reson. Imaging 36, 344–354. https://doi.org/10.1002/jmri.23670.
Liang, X., Tournier, J.-D., Masterton, R., Connelly, A., Calamante, F., 2012. A k-space sharing 3d grase pseudocontinuous ASL method for whole-brain resting-state functional connectivity. Int. J. Imaging Syst. Technol. 22, 37–43. https://doi.org/10.1002/ima.22006.
Liu, D., Duan, S., Zhou, C., Wei, P., Chen, L., Yin, X., Zhang, J., Wang, J., 2018. Altered brain functional hubs and connectivity in type 2 diabetes mellitus patients: a resting-state fMRI study. Front. Aging Neurosci. 10. https://doi.org/10.3389/fnagi.2018.00055.
Liu, H., Stufflebeam, S.M., Sepulcre, J., Hedden, T., Buckner, R.L., 2009. Evidence from intrinsic activity that asymmetry of the human brain is controlled by multiple factors. Proc. Natl. Acad. Sci. Unit. States Am. 106, 20499–20503. https://doi.org/10.1073/pnas.0908073106.
Liu, Z., Xu, C., Xu, Y., Wang, Y., Zhao, B., Lv, Y., Cao, X., Zhang, K., Du, C., 2010. Decreased regional homogeneity in insula and cerebellum: a resting-state fMRI study in patients with major depression and subjects at high risk for major depression. Psychiatry Res. Neuroimaging. 182, 211–215. https://doi.org/10.1016/j.pscychresns.2010.03.004.
Lu, H., Golay, X., Pekar, J.J., Van Zijl, P.C.M., 2003. Functional magnetic resonance imaging based on changes in vascular space occupancy. Magn. Reson. Med. 50, 263–274. https://doi.org/10.1002/mrm.10519.
Lu, H., Van Zijl, P.C.M., 2005. Experimental measurement of extravascular parenchymal BOLD effects and tissue oxygen extraction fractions using multi-echo VASO fMRI at 1.5 and 3.0 T. Magn. Reson. Med. 53, 808–816. https://doi.org/10.1002/mrm.20379.
Mantini, D., Perrucci, M.G., Gratta, C.D., Romani, G.L., Corbetta, M., 2007. Electrophysiological signatures of resting state networks in the human brain. Proc. Natl. Acad. Sci. Unit. States Am. 104, 13170–13175. https://doi.org/10.1073/pnas.0700668104.
Menon, V., 2011. Large-scale brain networks and psychopathology: a unifying triple network model. Trends Cognit. Sci. 15, 483–506. https://doi.org/10.1016/j.tics.2011.08.003.
Merola, A., Germuska, M.A., Murphy, K., Wise, R.G., 2018. Assessing the repeatability of absolute CMRO2, OEF and haemodynamic measurements from calibrated fMRI. Neuroimage 173, 113–126. https://doi.org/10.1016/j.neuroimage.2018.02.020.
Merola, A., Germuska, M.A., Warnert, E.A., Richmond, L., Helme, D., Khot, S., Murphy, K., Rogers, P.J., Hall, J.E., Wise, R.G., 2017. Mapping the pharmacological modulation of brain oxygen metabolism: the effects of caffeine on absolute CMRO2 measured using dual calibrated fMRI. Neuroimage 155, 331–343. https://doi.org/10.1016/j.neuroimage.2017.03.028.
Miao, X., Gu, H., Yan, L., Lu, H., Wang, D.J.J., Zhou, X.J., Zhuo, Y., Yang, Y., 2014. Detecting resting-state brain activity by spontaneous cerebral blood volume fluctuations using whole brain vascular space occupancy imaging. Neuroimage 84, 575–584. https://doi.org/10.1016/j.neuroimage.2013.09.019.
Miyata, M., Kakeda, S., Kudo, K., Iwata, S., Tanaka, Y., Wang, Y., Korogi, Y., 2018. Evaluation of oxygen extraction fraction in systemic lupus erythematosus patients using quantitative susceptibility mapping. J. Cereb. Blood Flow Metab. https://doi.org/10.1177/0271678X18764829.
Ogawa, S., Menon, R.S., Tank, D.W., Kim, S.G., Merkle, H., Ellermann, J.M., Ugurbil, K., 1993. Functional brain mapping by blood oxygenation level-dependent contrast magnetic resonance imaging. A comparison of signal characteristics with a biophysical model. Biophys. J. 64, 803–812. https://doi.org/10.1016/S0006-3495(93)81441-3.
Paakki, J.-J., Rahko, J., Long, X., Moilanen, I., Tervonen, O., Nikkinen, J., Starck, T., Remes, J., Hurtig, T., Haapsamo, H., Jussila, K., Kuusikko-Gauffin, S., Mattila, M.-L., Zang, Y., Kiviniemi, V., 2010. Alterations in regional homogeneity of resting-state brain activity in autism spectrum disorders. Brain Res. 1321, 169–179. https://doi.org/10.1016/j.brainres.2009.12.081.
Pannunzi, M., Hindriks, R., Bettinardi, R.G., Wenger, E., Lisofsky, N., Martensson, J., Butler, O., Filevich, E., Becker, M., Lochstet, M., Kühn, S., Deco, G., 2017. Resting-state fMRI correlations: from link-wise unreliability to whole brain stability. Neuroimage 157, 250–262. https://doi.org/10.1016/j.neuroimage.2017.06.006.
Patriat, R., Molloy, E.K., Meier, T.B., Kirk, G.R., Nair, V.A., Meyerand, M.E., Prabhakaran, V., Birn, R.M., 2013a. The effect of resting condition on resting-state fMRI reliability and consistency: a comparison between resting with eyes open, closed, and fixated. Neuroimage 78, 463–473. https://doi.org/10.1016/j.neuroimage.2013.04.013.
Patriat, R., Molloy, E.K., Meier, T.B., Kirk, G.R., Nair, V.A., Meyerand, M.E., Prabhakaran, V., Birn, R.M., 2013b. The effect of resting condition on resting-state fMRI reliability and consistency: a comparison between resting with eyes open, closed, and fixated. Neuroimage 78, 463–473. https://doi.org/10.1016/j.neuroimage.2013.04.013.
Raichle, M.E., MacLeod, A.M., Snyder, A.Z., Powers, W.J., Gusnard, D.A., Shulman, G.L., 2001. A default mode of brain function. Proc. Natl. Acad. Sci. Unit. States Am. 98, 676–682. https://doi.org/10.1073/pnas.98.2.676.

Rousson, V., Gasser, T., Seifert, B., 2002. Assessing intrarater, interrater and test–retest reliability of continuous measurements. Stat. Med. 21, 3431–3446. https://doi.org/10.1002/sim.1253.

Salvador, R., Suckling, J., Coleman, M.R., Pickard, J.D., Menon, D., Bullmore, E., 2005. Neurophysiological architecture of functional magnetic resonance images of human brain. Cerebr. Cortex 15, 1332–1342. https://doi.org/10.1093/cercor/bhi016.

Shehzad, Z., Kelly, A.M.C., Reiss, P.T., Gee, D.G., Gotimer, K., Uddin, L.Q., Lee, S.H., Margulies, D.S., Roy, A.K., Biswal, B.B., Petkova, E., Castellanos, F.X., Milham, M.P., 2009. The resting brain: unconstrained yet reliable. Cerebr. Cortex 19, 2209–2229. https://doi.org/10.1093/cercor/bhn256.

Shinn, A.K., Baker, J.T., Cohen, B.M., Öngür, D., 2013. Functional connectivity of left Heschl's gyrus in vulnerability to auditory hallucinations in schizophrenia. Schizophr. Res. 143, 260–268. https://doi.org/10.1016/j.schres.2012.11.037.

Smith, S.M., Fox, P.T., Miller, K.L., Glahn, D.C., Fox, P.M., Mackay, C.E., Filippini, N., Watkins, K.E., Toro, R., Laird, A.R., Beckmann, C.F., 2009. Correspondence of the brain's functional architecture during activation and rest. Proc. Natl. Acad. Sci. Unit. States Am. 106, 13040–13045. https://doi.org/10.1073/pnas.0905267106.

Song, X.-W., Dong, Z.-Y., Long, X.-Y., Li, S.-F., Zuo, X.-N., Zhu, C.-Z., He, Y., Yan, C.-G., Zang, Y.-F., 2011. Rest: a toolkit for resting-state functional magnetic resonance imaging data processing. PLoS One 6 e25031. https://doi.org/10.1371/journal.pone.0025031.

Stone, A.J., Blockley, N.P., 2017. A streamlined acquisition for mapping baseline brain oxygenation using quantitative BOLD. Neuroimage 147, 79–88. https://doi.org/10.1016/j.neuroimage.2016.11.057.

Stout, J.N., Adalsteinsson, E., Rosen, B.R., Bolar, D.S., 2018. Functional oxygen extraction fraction (OEF) imaging with turbo gradient spin echo QUIXOTIC (Turbo QUIXOTIC). Magn. Reson. Med. 79, 2713–2723. https://doi.org/10.1002/mrm.26947.

Tang, C., Wei, Y., Zhao, J., Nie, J., 2018. Different developmental pattern of brain activities in adhd: a study of resting-state fMRI. Dev. Neurosci. 40, 246–257. https://doi.org/10.1159/000490289.

Vincent, J.L., Kahn, I., Snyder, A.Z., Raichle, M.E., Buckner, R.L., 2008. Evidence for a frontoparietal control system revealed by intrinsic functional connectivity. J. Neurophysiol. 100, 3328–3342. https://doi.org/10.1152/jn.90355.2008.

Wang, J. -j., Chen, X., Sah, S.K., Zeng, C., Li, Y. -m., Li, N., Liu, M. -q., Du, S. -l., 2016. Amplitude of low-frequency fluctuation (ALFF) and fractional ALFF in migraine patients: a resting-state functional MRI study. Clin. Radiol. 71, 558–564. https://doi.org/10.1016/j.crad.2016.03.004.

Watchmaker, J.M., Juttukonda, M.R., Davis, L.T., Scott, A.O., Faraco, C.C., Gindville, M.C., Jordan, L.C., Cogswell, P.M., Jefferson, A.L., Kirshner, H.S., Donahue, M.J., 2016. Hemodynamic mechanisms underlying elevated oxygen extraction fraction (OEF) in moyamoya and sickle cell anemia patients. J. Cereb. Blood Flow Metab. https://doi.org/10.1177/0271678X16682509.

Weir, J.P., 2005. Quantifying test-retest reliability using the intraclass correlation coefficient and the SEM. J. Strength Cond. Res. 19, 231–240 .

Wu, C.W., Gu, H., Lu, H., Stein, E.A., Chen, J.-H., Yang, Y., 2009a. Mapping functional connectivity based on synchronized CMRO2 fluctuations during the resting state. Neuroimage 45, 694–701. https://doi.org/10.1016/j.neuroimage.2008.12.066.

Wu, T., Long, X., Zang, Y., Wang, L., Hallett, M., Li, K., Chan, P., 2009b. Regional homogeneity changes in patients with Parkinson's disease. Hum. Brain Mapp. 30, 1502–1510. https://doi.org/10.1002/hbm.20622.

Yablonskiy, D.A., Haacke, E.M., 1994. Theory of NMR signal behavior in magnetically inhomogeneous tissues: the static dephasing regime. Magn. Reson. Med. 32, 749–763. https://doi.org/10.1002/mrm.1910320610.

Yan, C.-G., Cheung, B., Kelly, C., Colcombe, S., Craddock, R.C., Di Martino, A., Li, Q., Zuo, X.-N., Castellanos, F.X., Milham, M.P., 2013. A comprehensive assessment of regional variation in the impact of head micromovements on functional connectomics. Neuroimage 76, 183–201. https://doi.org/10.1016/j.neuroimage.2013.03.004.

Yin, Y., Zhang, Y., Gao, J.-H., 2018. Dynamic measurement of oxygen extraction fraction using a multiecho asymmetric spin echo (MASE) pulse sequence. Magn. Reson. Med. 80, 1118–1124. https://doi.org/10.1002/mrm.27078.

Yu, R., Chien, Y.-L., Wang, H.-L.S., Liu, C.-M., Liu, C.-C., Hwang, T.-J., Hsieh, M.H., Hwu, H.-G., Tseng, W.-Y.I., 2014. Frequency-specific alternations in the amplitude of low-frequency fluctuations in schizophrenia. Hum. Brain Mapp. 35, 627–637. https://doi.org/10.1002/hbm.22203.

Zang, Y., Jiang, T., Lu, Y., He, Y., Tian, L., 2004. Regional homogeneity approach to fMRI data analysis. Neuroimage 22, 394–400. https://doi.org/10.1016/j.neuroimage.2003.12.030.

Zhang, D., Raichle, M.E., 2010. Disease and the brain's dark energy. Nat. Rev. Neurol. 6, 15–28. https://doi.org/10.1038/nrneurol.2009.198.

Zhou, Y., Shu, N., Liu, Y., Song, M., Hao, Y., Liu, H., Yu, C., Liu, Z., Jiang, T., 2008. Altered resting-state functional connectivity and anatomical connectivity of hippocampus in schizophrenia. Schizophr. Res. 100, 120–132. https://doi.org/10.1016/j.schres.2007.11.039.

Zhu, L., Fan, Y., Zou, Q., Wang, J., Gao, J.-H., Niu, Z., 2014. Temporal reliability and lateralization of the resting-state language network. PLoS One 9 e85880. https://doi.org/10.1371/journal.pone.0085880.

Zou, Q., Miao, X., Liu, D., Wang, D.J.J., Zhuo, Y., Gao, J.-H., 2015. Reliability comparison of spontaneous brain activities between BOLD and CBF contrasts in eyes-open and eyes-closed resting states. Neuroimage 121, 91–105. https://doi.org/10.1016/j.neuroimage.2015.07.044.

Zou, Q., Wu, C.W., Stein, E.A., Zang, Y., Yang, Y., 2009. Static and dynamic characteristics of cerebral blood flow during the resting state. Neuroimage 48, 515–524. https://doi.org/10.1016/j.neuroimage.2009.07.006.

Zou, Q., Zhou, S., Xu, J., Su, Z., Li, Y., Ma, Y., Sun, H., Wu, C.W., Gao, J.-H., 2018. Dissociated resting-state functional networks between the dream recall frequency and REM sleep percentage. Neuroimage 174, 248–256. https://doi.org/10.1016/j.neuroimage.2018.03.015.

Zou, Q.-H., Zhu, C.-Z., Yang, Y., Zuo, X.-N., Long, X.-Y., Cao, Q.-J., Wang, Y.-F., Zang, Y.-F., 2008. An improved approach to detection of amplitude of low-frequency fluctuation (ALFF) for resting-state fMRI: fractional ALFF. J. Neurosci. Methods 172, 137–141. https://doi.org/10.1016/j.jneumeth.2008.04.012.

Zuo, X.-N., Di Martino, A., Kelly, C., Shehzad, Z.E., Gee, D.G., Klein, D.F., Castellanos, F.X., Biswal, B.B., Milham, M.P., 2010a. The oscillating brain: complex and reliable. Neuroimage 49, 1432–1445. https://doi.org/10.1016/j.neuroimage.2009.09.037.

Zuo, X.-N., Kelly, C., Adelstein, J.S., Klein, D.F., Castellanos, F.X., Milham, M.P., 2010b. Reliable intrinsic connectivity networks: test–retest evaluation using ICA and dual regression approach. Neuroimage 49, 2163–2177. https://doi.org/10.1016/j.neuroimage.2009.10.080.

Zuo, X.-N., Kelly, C., Adelstein, J.S., Klein, D.F., Castellanos, F.X., Milham, M.P., 2010c. Reliable intrinsic connectivity networks: test–retest evaluation using ica and dual regression approach. Neuroimage 49, 2163–2177. https://doi.org/10.1016/j.neuroimage.2009.10.080.

Zuo, X.-N., Xing, X.-X., 2014. Test-retest reliabilities of resting-state fMRI measurements in human brain functional connectomics: a systems neuroscience perspective. Neurosci. Biobehav. Rev. 45, 100–118. https://doi.org/10.1016/j.neubiorev.2014.05.009.

Zuo, X.-N., Xu, T., Jiang, L., Yang, Z., Cao, X.-Y., He, Y., Zang, Y.-F., Castellanos, F.X., Milham, M.P., 2013. Toward reliable characterization of functional homogeneity in the human brain: preprocessing, scan duration, imaging resolution and computational space. Neuroimage 65, 374–386. https://doi.org/10.1016/j.neuroimage.2012.10.017.